Journal of Catalysis 299 (2013) 188–203

Contents lists available at SciVerse ScienceDirect

Journal of Catalysis

journal homepage: www.elsevier.com/locate/jcat

Structure and critical function of Fe and acid sites in Fe-ZSM-5 in propane oxidative dehydrogenation with N_2O and N_2O decomposition

Petr Sazama *, Naveen K. Sathu, Edyta Tabor, Blanka Wichterlová, Štěpán Sklenák, Zdeněk Sobalík

J. Heyrovský Institute of Physical Chemistry, Academy of Sciences of the Czech Republic, CZ-182 23, Prague 8, Czech Republic

ARTICLE INFO

Article history:
Received 22 August 2012
Revised 27 November 2012
Accepted 9 December 2012

Keywords:
Fe-ZSM-5 zeolite
Structure of Fe species
Steamed Fe-zeolites
Mössbauer spectroscopy
UV–Vis
FTIR
H_2-TPR
N_2O decomposition
Propane oxidative dehydrogenation by N_2O

ABSTRACT

The structure and population of ion-exchanged Fe ions, Fe-oxo species, and Fe-oxo oligomers and Fe_2O_3 oxide particles and the concentration of acid sites in non-steamed and steamed Fe-ZSM-5 were elucidated using semi-quantitative Mössbauer and FTIR analysis supplemented by UV–Vis and H_2-TPR. Differences in the concentration of the individual Fe species and acid sites were related to the activity and time-on-stream behavior of Fe-zeolites in decomposition of N_2O and oxidative dehydrogenation of propane to propene with N_2O. The evacuated non-steamed FeH-ZSM-5 contained high concentration of Brønsted sites and predominantly bare Fe(II) ions (72%), and less mono- and dinuclear Fe(III) (16–19%) and oligomeric Fe(III)-oxo species (9–12%). The steamed Fe(H)-ZSM-5st zeolites were greatly reorganized, resulting in a low concentration of both the Brønsted sites and bare Fe(II) ions, and the T_d-coordinated Fe(III) ions in the Fe—Al—Si extra-framework species (43–47%) and Fe-oxide-like particles (30–33%) prevailed. The redox state of Fe in both non-steamed and steamed Fe-ZSM-5 was strongly influenced by the reaction conditions of N_2O decomposition and C_3H_8/N_2O. Bare counter Fe ions balanced by Al—Si—Si—Al sequences in 6MRs of the framework undergo reversible redox $Fe(III)O^-/Fe(II)$ cycle during N_2O/evacuation treatments and represent the most active site in the decomposition of N_2O to molecular components. In contrast, both mono-, dinuclear Fe(III)-oxo and Fe(III)-oxo oligomers are reduced by propane to Fe(II) at conditions of the C_3H_8/N_2O reaction. The reduced Fe(II) species with N_2O form $Fe(III)—O^-$ and facilitate transfer of atomic oxygen to propane with formation of propanol dehydrated to propene. Thus, all dispersed Fe species represent highly active sites in oxidative dehydrogenation of propane to propene with N_2O. The presence of high concentration of Brønsted sites and large crystal size of FeH-ZSM-5 stimulated oligomerization of formed propene decreasing its yield and increasing retention of polyolefins up to polyaromatic coke. Thus, high concentration of counter Fe(III)-oxo species easily reducible to Fe(II) is critical for high activity in N_2O decomposition, whereas high yield of propene in C_3H_8/N_2O is achieved regardless of population of the individual dispersed Fe species. The low concentration of protonic sites and small crystallites of zeolites, not supporting propene oligomerization, accumulation of polyolefins in the pores and their easy oxidation to CO/CO_2, are necessary conditions for selective oxidative dehydrogenation of propane to propene over Fe-ZSM-5.

1. Introduction

The interaction between N_2O and Fe(II) ions stabilized in the extra-framework sites of high-silica zeolites results in N_2O dissociation and formation of the so-called α-oxygen bound to Fe ions and gaseous nitrogen. These α-oxygen atoms either recombine or interact with an additional N_2O molecule with formation of molecular oxygen [1] or can be used for highly selective oxidations of hydrocarbons, such as benzene to phenol [2–7], methane to methanol [8,9], and propane to propene via propanol [10–14] according to the following pathways:

$$Fe(II) + N_2O \rightarrow Fe(III)—O^- + N_2 \quad (1)$$

$$Fe(III)—O^- + Fe(III)—O^- \rightarrow 2Fe(II) + O_2 \quad (2)$$

$$Fe(III)—O^- + N_2O \rightarrow Fe(II) + N_2 + O_2 \quad (3)$$

or

$$Fe(III)—O^- + C_3H_8 \rightarrow Fe(II) + C_3H_7OH \rightarrow Fe(II) + C_3H_6 + H_2O \quad (4)$$

The high reactivity of this atomic oxygen bound to Fe(III) ions suggests the radical-type character of the $Fe(III)—O^-$ species, although there is so far no direct experimental evidence for it. In addition to investigation into the reactivity of α-oxygen itself [7,15–18], there is continuous interest in analysis of the structures of Fe sites, particularly in ZSM-5 and ferrierite, responsible for the activity in

---

* Corresponding author.
E-mail address: petr.sazama@jh-inst.cas.cz (P. Sazama).

0021-9517/$ - see front matter © 2012 Elsevier Inc. All rights reserved.
http://dx.doi.org/10.1016/j.jcat.2012.12.010

selective oxidation of hydrocarbons as well as N_2O decomposition to molecular components. Accordingly, two competitive processes, N_2O decomposition to molecular products, employed for N_2O abatement at end-of-pipe gases of nitric acid plants and selective oxidation of hydrocarbons of low reactivity exploiting the high reactivity of oxygen bound on Fe sites, are at the center of attention.

Dinuclear μ-oxo Fe complexes in ZSM-5, formed by high-temperature calcination or steaming of the originally isomorphously substituted [Fe]ZSM-5 with Fe ions removed from the framework or introduced by ion exchange, were suggested to be the active sites in the hydroxylation of benzene [1,19–26]. This suggestion was based mainly on the Mössbauer spectra of the iron-exchanged Fe-ZSM-5 and steamed isomorphously substituted [Fe]ZSM-5 zeolites yielding similar Mössbauer parameters to those of the dinuclear Fe-oxo complexes of methane monooxygenase [1,27]. EXAFS experiments also indicated the presence of dinuclear Fe complexes mostly in the highly loaded Fe-zeolites with Fe/Al composition ~1 [20,26–30]. Later, it was shown that both the Fe ions of the dinuclear complex and single Fe(II) ions in cationic sites of ZSM-5 and ferrierite bind one α-oxygen, thus forming an $Fe(III){-}O^{-}$ entity [1]. On the other hand, structurally undefined (but related to the Al presence) Fe—Si—Al—O species [31] formed in the pores of steamed [FeAl]ZSM-5 were also suggested as the highly active centers for oxidation of benzene to phenol. Although the steaming of both the isomorphously substituted H-[Fe]ZSM-5 and the ion-exchanged FeH-ZSM-5 appeared to be accompanied by substantial changes in the structure of the Fe species and to be beneficial for yields of phenol and also resulted in a lower rate of catalyst deactivation [2,3], the elucidation of the structure of the active Fe sites in the steamed FeH-zeolites is still far from being resolved.

Oxidative dehydrogenation of propane to propene by nitrous oxide over the ion-exchanged FeH-ZSM-5 with interesting yields of propene has also been reported [11,19,32]. The importance of the Fe ions balanced by the negative framework charge was pointed out [33], but no conclusion was drawn on the structure of the active Fe sites, except for the statement that the highest TOF values are reached at the lowest (even trace) concentrations of Fe. On the other hand, with N_2O decomposition, in addition to the dinuclear Fe-oxo complexes, the exchanged single Fe(II) ions were clearly shown to be the active sites [34,35]. Different distances of the Fe(II) ions at defined cationic sites for low concentrations of Fe in MFI, FER, and BEA zeolite structures have been indicated to control the rate of decomposition of nitrous oxide to molecular products [34]. Very specific complex structure in the low-loaded Fe-FER including two Fe ions facing each other in the opposite β-type cationic sites was proposed for N_2O decomposition [36]. As this thus-define distance could not be realized in ZSM-5 structure due to different arrangement of the β-type six-member rings (6MRs) coordinated Fe(II) ions, the N_2O decomposition activity of Fe-ZSM-5 compared to Fe-FER is lower [34]. These suggestions were supported by the results of DFT calculations describing the individual steps of N_2O interaction with two Fe(II) ions located in cationic sites. The recombination of oxygen atoms or their reaction with additional N_2O was suggested as the rate-determining step [7,37].

The structural chemistry of iron in high-silica zeolites is very complex. Single, di,- and trivalent Fe ions, mono- and dinuclear oxo- and hydroxo-complexes, oligomeric oxo species and iron oxide particles coexist in various proportions depending on the Fe loading, methods of Fe introduction and also the zeolite structure [25,34,38–41]. Fe-zeolites with highly predominant single Fe ions in cationic sites were prepared only at low loadings, while higher loadings immediately exhibit a variety of Fe species [42]. XANES and EXAFS studies of the highly loaded Fe-ZSM-5 prepared by sublimation of $FeCl_3$ clearly evidenced presence of dinuclear Fe-oxo complexes [29,30,43]. All types of Fe species can be found in a diverse set of oxidation states and stereochemical conformations (tetrahedral, five-coordinated, trigonal bipyramid and six-coordinated [44], and the formation of oxo-bridged and di-oxo-bridged dimeric and oligomeric species up to bulk-like α-FeO(OH) and α-Fe_2O_3 [45,46]). The most complex view of the state of Fe is provided by Mössbauer spectroscopy whose parameters distinguish Fe(II) and Fe(III) ions and are sensitive to their coordination with oxygen-containing ligands [35,47–54]. Nevertheless, necessity of fitting the Mössbauer parameters from the complex spectra of the individual Fe(II)/Fe(III) species with different coordination makes the analysis of Fe complexes in Fe-zeolites only semi-quantitative. Pirngruber et al. [26] analyzing the monomeric, dimeric, and oligomeric Fe species in zeolites by UV–Vis, EXAFS, and magnetic susceptibility measurements, critically stressed the shortcomings of the individual methods. They concluded that the magnetic measurements supplemented by UV–Vis might provide semi-quantitative information on the nuclearity of the Fe sites, and they were skeptical about the use of EXAFS for quantitative analysis of mono- and dimeric Fe species.

The present work is focused on the structural analysis of two Fe ion-exchanged FeH-ZSM-5 zeolites of different crystal size with comparable low Fe concentrations ($Fe/Al \sim 0.15$ at $Si/Al \sim 22$) and their steamed forms by following their auto-reduction and interaction with molecular oxygen, N_2O, and propane/N_2O at the reaction temperature. The analysis of Fe-zeolites with respect to Fe species and acid sites is based on the ^{57}Fe Mössbauer (Fe(II)/Fe(III)) and FTIR spectroscopy of acid and Fe(II) sites, supported by temperature-programmed reduction by hydrogen (TPR-H_2) and the UV–Vis spectra of the Fe(III) ions. The activity of Fe-zeolites in competitive reactions of N_2O decomposition to molecular products and oxidative dehydrogenation of propane to propene with N_2O were related to the concentration of the Fe(II)/Fe(III) sites, the protonic sites, and the crystal size.

2. Experimental

2.1. Structure of parent zeolites

Parent Na-ZSM-5 zeolites with Si/Al molar ratio of 21.9 and 21.6, and crystal size 0.15 and 2 μm were designated as Z1 and Z2, respectively. The crystal size of the samples was estimated from the SEM micrographs (JEOL JSM-5500LV scanning electron microscope) given in Supplement I. The zeolite samples of different crystal size were selected to follow the accumulation of polyolefins inside pores during propane oxidation. Zeolites crystallinity was checked by XRD using a Bruker D8 (Bruker AXS, USA) diffractometer, and N_2 physisorption isotherms (77 K) were obtained by an ASAP2020 Micromeritics apparatus. The XRD patterns of parent zeolites were characteristic for the structure of ZSM-5 (Supplement II). N_2 adsorption isotherms indicated a well-developed micropore volume (0.15–0.16 $cm^3\,g^{-1}$) and an external surface area corresponding to the crystal size (Supplement III and Table 1). ^{27}Al MAS NMR spectra of the parent zeolites were measured by a Bruker Avance 500 MHz (11.7 T) Wide Bore spectrometer using 4 mm o.d. ZrO_2 rotors with a rotation speed of 12 kHz. Proton high-power decoupling pulse sequences with p/6 (1.4 μs) excitation pulses were employed to allow quantitative evolution of the ^{27}Al MAS NMR spectra. The ^{27}Al MAS NMR spectra of hydrated Na-ZSM-5 zeolites (Supplement IV) exhibited strong resonance with a chemical shift of about 55 ppm corresponding to the tetrahedrally coordinated Al atoms in the zeolite framework. Octahedral Al with a resonance of about 0 ppm was not observed. Table 1 gives the characteristics of NH_4-ZSM-5 obtained by the three-fold ion exchange of Na-zeolites with 0.5 M NH_4NO_3 at RT, and their steamed forms, (H)-ZSM-5st.

Table 1
Characteristics of parent H-ZSM-5 zeolites.

Sample	Si/Al	c_{Al}[a]	c_B[b] (mmol g^{-1})	c_L[c]	Crystal size (μm)	S_{BET} ($m^2\ g^{-1}$)	S_{EXT} ($m^2\ g^{-1}$)	V_{MI} ($cm^3\ g^{-1}$)
H-Z1	21.9	0.73	0.32 *(0.04)*	0.14 *(0.06)*	0.15	382	47	0.15
H-Z2	21.6	0.74	0.43 *(0.05)*	0.09 *(0.07)*	2	358	11	0.16

In brackets – after treatment in a stream of 30% H_2O and 35% O_2 in He at 600 °C for 4 h.
[a] From chemical analysis.
[b] Concentrations of Brønsted sites from FTIR spectra of adsorbed d_3-acetonitrile.
[c] Concentrations of Lewis sites from FTIR spectra of adsorbed d_3-acetonitrile.

Table 2
Chemical composition, concentration of Brønsted and Lewis acid sites, and Fe(II) in Fe-ZSM-5 zeolites.

Zeolite	c_{Fe}[a] (wt.%)	Fe/Al[a]	Crystal size (μm)	c_B[b] (mmol g^{-1})	c_L[c] (mmol g^{-1})	$c_{Fe(II)}$[d] (mmol g^{-1})
FeH-Z1	0.69	0.17	0.15	0.26	0.09	0.09
Fe(H)-Z1st				0.05	0.04	0.02
FeH-Z2	0.59	0.14	2	0.31	0.04	0.08
Fe(H)-Z2st				0.05	0.03	0.02

[a] From chemical analysis.
[b] Concentration of Brønsted sites from FTIR spectra of adsorbed d_3-acetonitrile.
[c] Concentration of Lewis sites from FTIR spectra of adsorbed d_3-acetonitrile.
[d] Concentration of Fe(II) ions in cationic sites from FTIR spectra of adsorbed d_3-acetonitrile.

2.2. Preparation of Fe-zeolites

Fe was introduced into NH_4-zeolites by their impregnation with anhydrous $FeCl_3$ in acetylacetone, following calcination and hydrolysis (for details see Ref. [34]). The samples are referred to as FeH-Z1 and FeH-Z2 (Table 2). Parts of the calcined Fe-samples were steamed at 600 °C for 4 h in a stream of 30% water vapor and 35% O_2 in He and denoted as Fe(H)-Z1st and Fe(H)-Z2st (Table 2). The Fe-zeolites for the Mössbauer spectroscopy measurement of the same chemical composition (^{57}FeH-Z1 and ^{57}FeH-Z2) were prepared from identical parent NH_4-zeolites using the same procedure employing isotopically enriched $^{57}FeCl_3$ (>96%). Steaming of the isotopically enriched ^{57}Fe-zeolites was also performed under the same conditions.

2.3. Structural analysis of Fe-zeolites

The chemical compositions of the Fe-zeolites were determined by X-ray fluorescence spectroscopy using a PW 1404 (Philips) instrument. The FTIR spectra of the zeolites evacuated at 450 °C were recorded at RT on a Nicolet Nexus 670 FTIR spectrometer equipped with a MCT-B detector operating at 2 cm^{-1} resolution by collecting 200 scans for a single spectrum. The concentration of acidic Brønsted and Lewis sites in H-ZSM-5 and Fe(II) sites in Fe-zeolites was determined by the adsorption of d_3-acetonitrile at RT on the evacuated zeolites from the intensities of the characteristic IR bands of the C≡N vibrations. The extinction coefficients for the corresponding C≡N vibrations were taken from Ref. [55]. The UV–Vis spectra of the dehydrated Fe-zeolites were measured in the range from 4000 to 50,000 cm^{-1} using a Perkin-Elmer Lambda 950 spectrometer equipped with a Spectralon™ integration sphere, also used as a reference. The samples were dehydrated at 100 °C for 30 min and evacuated at 450 °C for 3 h. The spectra were processed according to the Schuster–Kubelka–Munk equation: $F(R_\infty) = (1 - F(R_\infty))^2/2R_\infty$. H_2-TPR experiments were carried out using an Altamira AMI 200 instrument. Prior to the H_2-TPR analysis, the Fe-zeolites were dehydrated in a stream of air at 450 °C for 1 h. The N_2O pre-treatment, if employed, was performed at 200 or 400 °C on the dehydrated zeolites. The reduction in Fe-zeolites by hydrogen was carried out in an H_2/Ar stream (9.44 vol.% H_2) at a total flow rate of 30 ml min^{-1} and linear heating rate of 10 °C min^{-1} up to 800 °C. Mössbauer spectroscopy measurements were carried out on ~100 mg self-supporting pellets (10 mm in diameter) of ^{57}Fe-ZSM-5 placed in a laboratory-made chamber. Mössbauer spectra were collected at RT on samples after (i) evacuation at 450 °C for 3 h, following interaction with (ii) O_2 at 450 °C for 30 min and evacuation at 450 °C for 5 min, or (iii) N_2O at 400 °C for 30 min and evacuation at 400 °C for 5 min, or (iv) with propane/N_2O (1:1 molar) followed by evacuation at 400 °C for 5 min. ^{57}Co in an Rh matrix was used as a source of γ rays. The maximum velocity of the source was 12 mm s^{-1}; the velocity scale was calibrated by α-Fe. The spectra were deconvoluted into Lorentzian-shaped components using the MossWinn software. The components were characterized by the Mössbauer parameters, the isomer shift (IS), and quadrupole splitting (QS) providing for the valence state and coordination, respectively.

2.4. Catalytic experiments

Oxidation of propane with nitrous oxide over Fe-zeolites was carried out in a bed-plug flow-through quartz micro-reactor (I.D. = 4 mm) with 50 mg of the catalyst (grains of 0.3–0.6 mm) pre-treated at 450 °C in a stream of He (50 ml min^{-1}) for 30 min. The reaction mixture, consisting of 1.5% N_2O and 1.5% C_3H_8 in He, was maintained at a total flow rate of 100 ml min^{-1} with corresponding WHSV 3.5 h^{-1}. The reactant and product gas compositions were analyzed using a combination of an online-connected GC (HP 6890) and a quadrupole mass spectrometer (Pfeiffer OmniStar, GSD 301 C). Two gaseous samples were simultaneously injected through 10-port valves into two branches of a GC equipped with a thermal conductivity detector (TCD) and a flame ionization detector (FID). In the first branch, an HP-PLOT Q capillary column (30 m, 0.53 mm × 40 μm film thickness) and an FID were used for analysis of the hydrocarbons. A TCD and Hysep column (packed column), a HP-Plot Q column (30 m, 0.53 mm × 40 μm film thickness), and a molecular sieve 5A column (30 m, 0.53 mm × 25 μm film thickness) were used for the analysis of O_2, N_2, N_2O, CO, and CO_2 in the second branch. The Hysep column was used for the retention and removal of organic compounds and water. In addition to propene, CO and CO_2 as the major products, small quantities of methane, ethane, ethene, traces of butanes, butenes, and benzene were found. As the yields of these products were typically below 1%, they are not reported in the results. Temperature-programmed oxidation (TPO) was used for analysis of the hydrocarbon deposits on the catalysts during the reaction after time-on-stream (TOS) of 4 h. A mixture of 50% O_2 in He with a total flow rate of 50 ml min^{-1} was employed at an increasing temperature yielding CO, CO_2, and H_2O continuously monitored by an online-connected mass spectrometer (Pfeiffer OmniStar, GSD 301 C). The carbon balance based on the mass of propane converted and the sum of the products (C_1—C_6 hydrocarbons, CO, CO_2 and coke deposits) was within the 10% uncertainty interval. The nature and amount of hydrocarbon residues deposited on the catalysts after TOS of 240 min were estimated by temperature-programmed oxidation in an oxygen stream from 25 to 650 °C.

The N_2O decomposition was followed at 400 and 425 °C using a U-shaped flow-through reactor. Before the test, the catalyst (50 mg, 0.3–0.6 mm) was pre-treated *in situ* in a helium stream at 450 °C for 2 h, followed by its treatment in an oxygen stream for 1 h at the same temperature. The flow rate of nitrous oxide (1000 ppm) in He as a carrier gas was 300 cm^3 min^{-1}, corresponding to GHSV of 180,000 h^{-1}. Analysis of the gas composition at the reactor outlet was performed using an Advance Optima IR analyzer (ABB Co., Germany).

To check if the reactions take place in a kinetic regime, a catalyst weight of 17 mg, carrier gas flow of 100 cm^3 min^{-1}, and N_2O concentration of 1000 ppm, that is, the identical GHSV 180,000 h^{-1} were used. The obtained N_2O conversions over FeH-Z2 (2.1% and 4.8% at 400 and 425 °C, cf. Table 6) showed absence of external mass and heat transfer. As for the mass transfer inside the crystals, the close values of TOF per Fe for N_2O decomposition (7.2×10^{-4} and 9.3×10^{-4} s^{-1}, respectively) and propane oxidation (0.054 and 0.064 s^{-1}, resp.) at 400 °C, and similar distribution of Fe species in Fe-HZ1 and FeH-Z2 samples (see the structure analysis in Section 3.3) excluded significant effect of intra-crystalline diffusion.

3. Results

3.1. FTIR spectra of FeH-ZSM-5 and Fe(H)-ZSM-5st

Fig. 1 shows the FTIR spectra in the region of hydroxyl group vibrations of H-ZSM-5 and FeH-ZSM-5 and after their steaming (all evacuated at 450 °C). The variable light scattering on crystals of different size could affect the intensities of the spectral components. Nevertheless, comparison of the band intensity of the individual samples before and after the Fe introduction and after the steaming enabled the analysis of the structural changes with respect to Fe and Al-related acid sites. The coordination of Fe ions to bridging oxygen atoms of the framework is documented by an intensity decrease in the band at 3610 cm^{-1} of the stretching vibration of the bridging hydroxyls, while the band of terminal silanols at 3745 cm^{-1} was unchanged (Fig. 1A). Steaming of FeH-zeolites at 600 °C at 30% water vapor produced a considerable loss of the bridging hydroxyls and partial loss of the terminal silanols. The decreased concentration of hydroxyls is consistent with the removal of Al from the framework with formation of extra-framework Al species and condensation of silanol groups. Low-intensity bands appearing at 3660 and 3786 cm^{-1} were ascribed to OH groups bound to perturbed framework Al atoms and extra-framework Al atoms or Fe ions and to OH groups on agglomerated Al_2O_3-type species [56,57]. As all these groups easily dehydroxylate, they cannot be used as a measure of the concentration of extra-framework Al and Fe species [57,58].

Adsorption of d_3-acetonitrile on the H-ZSM-5 and their steamed forms resulted in the complete disappearance of the band at 3610 cm^{-1} with the appearance of the bands at 2298 and 2325 cm^{-1} of the stretching vibrations of C≡N groups interacting with Brønsted and Al-Lewis sites, respectively (Fig. 1B). Their quantitative analysis using the extinction coefficients from Ref. [55] is given in Table 1. Parent H-ZSM-5 exhibited highly predominant Brønsted sites with low concentration of Lewis sites. The steaming at 600 °C led to a substantial decrease in the concentration of the Brønsted sites consistent with the release of Al from the framework.

d_3-Acetonitrile adsorbed on FeH-ZSM-5 and Fe(H)-ZSM-5st resembled Al-Lewis sites at 2325 cm^{-1} and the band with maximum around 2300 cm^{-1} (Fig. 1B), which was shifted to lower or higher frequencies depending on the relative concentration of the bridging SiOHAl groups and Fe ions. While the band at 2325 cm^{-1} reflected exclusively Al-Lewis sites, the band around 2300 cm^{-1} represented an overlap of the C≡N vibrations interacting with the Brønsted sites (2298 cm^{-1}) and Fe(II) ions behaving as electron-acceptor Lewis sites (2303 cm^{-1}). The individual frequencies were determined by the step-by-step desorption of d_3-acetonitrile occurring at increasing temperature preferably from the Brønsted SiOHAl sites (not shown). Supplement V shows deconvolution of the IR bands of the C≡N groups on Fe-zeolites. Both steamed Fe(H)-ZSM-5st zeolites exhibited a shift in the absorption maximum from 2300 to 2303 cm^{-1} and its much lower intensity compared to the FeH-zeolites. Thus, much lower concentrations of structural OH groups and bare Fe(II) ions were found in the Fe(H)-ZSM-5st in comparison with FeH-ZSM-5 zeolites. The estimated concentrations of SiOHAl, Fe(II) ions and Al-Lewis sites are given in Table 2; note that the extinction coefficients of C≡N interacting with Fe(II) and Al-Lewis sites are roughly twice those for compounds with Brønsted sites [59].

3.2. H_2-TPR

Figs. 2 and 3 compare the H_2-TPR profiles of the FeH-ZSM-5 and steamed Fe(H)-ZSM-5st zeolites pre-treated in a stream of air (450 °C) and after their interaction with N_2O at 200 and 400 °C. All FeH-ZSM-5 oxidized at 450 °C exhibited broad non-symmetrical hydrogen consumption from 250 up to 450 °C with maximum at about 400 °C. For both the steamed Fe(H)-ZSM-5st zeolites compared to FeH-ZSM-5, approximately twice as much hydrogen was consumed, and the reduction maximum was shifted from 400 to 460 °C. Both FeH-ZSM-5 after interaction with N_2O at temperatures as low as 200 °C (but not the steamed samples) exhibited a sharp peak at 230 °C, which was increased after N_2O interaction at 400 °C, and also appeared for the steamed zeolites (Fig. 2). At the same time, the hydrogen consumption in a broad region from 250 to 450 °C was practically not changed for the FeH-zeolites, but was considerably higher for steamed zeolites (Fig. 3). Nevertheless, the steamed zeolites exhibited lower intensity of the peak at 230 °C. These results indicate that various types of Fe species are present differing in their reactivity toward N_2O.

The Fe(II) ions coordinated in the cationic sites to framework oxygen atoms present in FeH-ZSM-5 (see the Mössbauer spectra analysis in Section 3.1.3) are highly stabilized and did not undergo reduction by hydrogen up to approximately 700 °C, and consequently, they are not reflected in the H_2-TPR experiments. The sharp reduction peak at 230 °C is attributed to the reduction in monoatomic oxygen from the Fe(III)—O^- species reduced to Fe(II) [34]. The significant reduction in Fe species in the broad region 250–450 °C was also observed for low-loaded Fe-FER and Fe-MFI with the Fe ions predominantly in cationic sites [34,60,61] This corresponds to the structural conditions for their oxidation by molecular oxygen, probably forming some di- and polynuclear Fe-oxo species. Hydrogen consumption in a broad temperature range indicates a variety in bonding of the Fe(III) species.

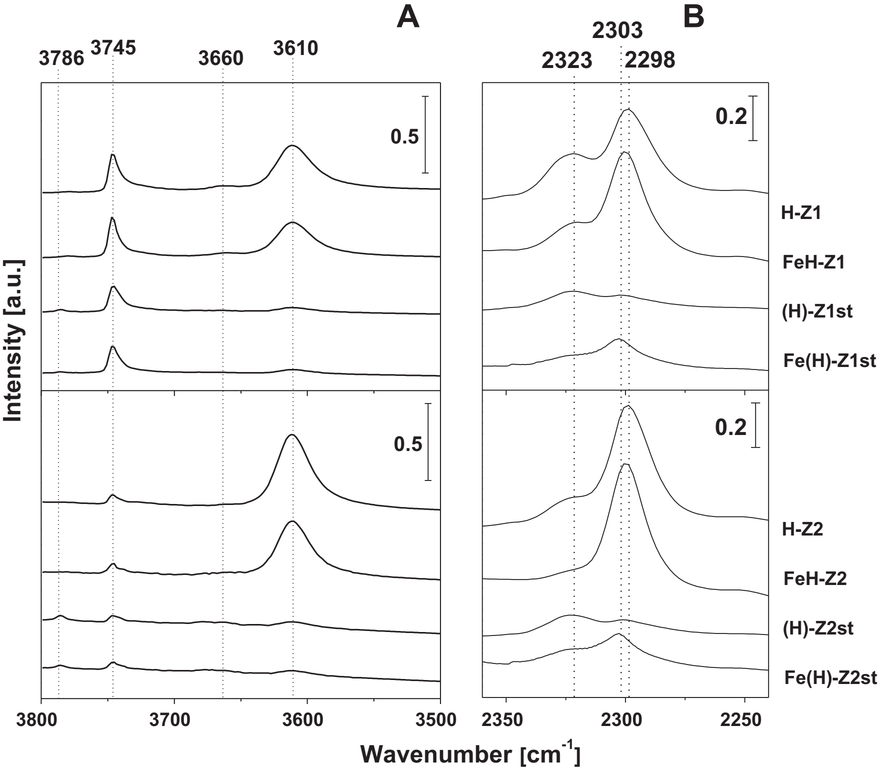

Fig. 1. FTIR spectra of H- and FeH-ZSM-5, and steamed (H)- and Fe(H)-ZSM-5st zeolites. (A) OH vibrations after evacuation at 450 °C, (B) C≡N vibrations after adsorption of d_3-acetonitrile (13 mbar) at RT and evacuation at RT.

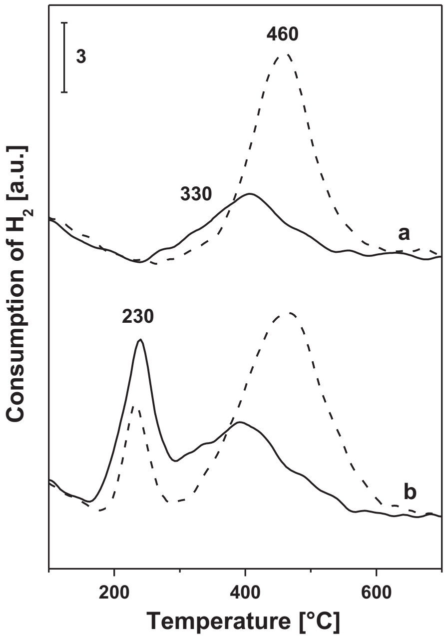

Fig. 2. Comparison of H_2-TPR profiles of FeH-Z2 (—) and steamed Fe(H)-Z2st (---) pre-treated in (a) air at 450 °C and (b) a stream of Ar at 450 °C followed by a stream of N_2O at 400 °C prior to the measurement.

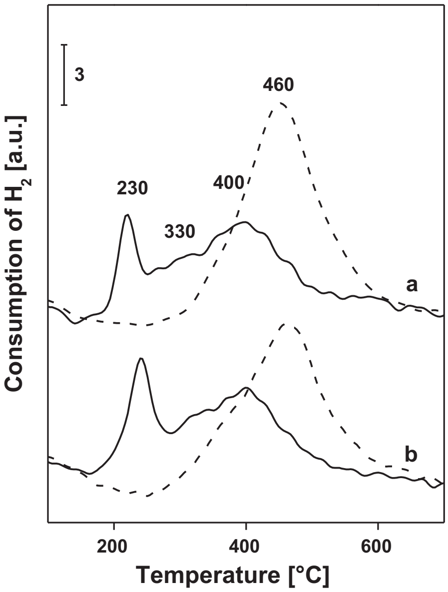

Fig. 3. Comparison of H_2-TPR profiles of FeH-ZSM-5 (–) and steamed Fe(H)-ZSM-5st (---) pre-treated in air at 450 °C, followed by interaction with N_2O at 200 °C prior to the measurement. (a) FeH-Z1 vs. Fe(H)-Z1st and (b) FeH-Z2 vs. Fe(H)-Z2st.

The shift in the temperature of hydrogen consumption to higher temperatures (max. 460 °C) and its doubling after the steaming of FeH-zeolites showed an increase in the concentration of the Fe(III) species with a lower tendency to be reduced (a decrease in the range of 300–400 °C). The broader range of reduction indicated a change in the Fe-oxo species nuclearity. A reduction temperature of up to 600 °C by hydrogen was also found by others for Fe-ZSM-5 with high Fe loading (~Fe/Al 1), presumably containing small Fe-oxide particles and Fe-loaded silica with supported Fe-oxo oligomers and dispersed Fe-oxide species [60].

It follows that the reduction peak of FeH-ZSM-5 zeolites at 230 °C reflects originally Fe(II) ions stabilizing monoatomic oxygen (Fe(III)—O$^-$) and the reductions at 300–400 °C of the Fe(III)-oxo ions in cationic sites, forming dinuclear Fe(III)—O_n—Fe(III) and small oligomeric Fe-oxo species. The zeolite steaming results in fewer Fe(II) ions capable of binding an oxygen atom from N_2O (Fe(III)—O^-) and also in a decrease in the population of Fe(III)—O_n—Fe(III) species connected with the cationic sites (300–400 °C), and an increase in polynuclear oligomeric Fe-oxo species and Fe-oxide-like species, reduced above 450 °C.

3.3. Mössbauer spectra

In the Mössbauer spectra of Fe-zeolites, the isomer shift (IS) and quadrupole splitting (QS) reflect the valence state and coordination of the high spin Fe(III) and Fe(II) complexes, respectively [1,35,47,52–54,62]. The Mössbauer spectra of the dehydrated (evacuated at 450 °C) FeH-ZSM-5 zeolites are presented in Supplement VI. The IS and QS parameters obtained by the spectral deconvolution using Lorentzian curves are listed in Table 3. The parameters with the best fit were obtained after the spectral decomposition into four components. Similar parameters obtained for two FeH-ZSM-5 samples of similar Fe/Al and Si/Al composition, differing only in the crystal size support the validity of the deconvolution. IS values between 0.7 and 1.4 mm s^{-1} were assigned to Fe(II), whereas those from 0.1 to 0.6 mm s^{-1} were suggested to correspond to Fe(III) ions [1,35,51,63,64]. Two components (D1, D2) exhibiting IS > 0.9 mm s^{-1} were attributed to Fe(II) ions. Their sum represents a dominant fraction of the total Fe content (72% for both FeH-Z1 and FeH-Z2). As the concentration of Fe in zeolites is low (Fe/Al 0.15), and the Mössbauer spectra of the dehydrated Fe-ferrierites with low Fe concentration yielded similar parameters for the Fe(II) ions (IS = 1.02 mm s^{-1}, QS = 2.02 mm s^{-1}; IS = 0.92 mm s^{-1} QS = 0.44 mm s^{-1}; IS = 0.94 mm s^{-1} QS = 0.70 mm s^{-1}), see Ref. [54], we assigned the D1 and D2 components in FeH-ZSM-5 (IS = 1.02 mm s^{-1} and QS = 2.35, 2.37 mm s^{-1} and IS = 0.92–0.93 mm s^{-1} and QS = 0.78 mm s^{-1}) to the Fe(II) ions in cationic sites balanced by two AlO_4^- tetrahedra in the ring. Most of the bare Fe(II) ions can be expected to be coordinated to the β-type 6MRs containing two Al atoms at the intersection of the main and sinusoidal channels of ZSM-5 and less at the α-type cationic site (note that here, the α-type 6MR does not mean the α-type oxygen atom of Panov) at the wall of the straight channel (for details on the siting of divalent cations in ZSM-5, see Ref. [65], and on the distribution of Al atoms in the framework controlling siting of divalent cations, see Ref. [66]). The D1 doublet with the higher QS (IS = 1.02 mm s^{-1} and QS = 2.37 and 2.35 mm s^{-1}), indicating lower symmetry of the Fe coordination, could be connected either with the bare Fe(II) ions located above the α-type 6MRs or more probably with some dinuclear oxygen bridged Fe(II)—O—Fe(II) species. The IS and QS parameters of the main D1 and D2 components of Fe(II) ions reported here (Table 3) are close to the Mössbauer parameters of Dubkov et al. [1] for Fe-ZSM-5 and to those of the Fe(II) ions in ferrierite, where the Fe(II) ions are coordinated to similar framework rings [35,67]. The low IS values of the D3 and D4 components (0.31 and 0.47 mm s^{-1}) correspond to the presence of Fe(III) species [1,51,53]. The high QS value of the D4 component (QS = 2.16 mm s^{-1}) indicates the presence of the low-symmetry Fe(III) species [35,51]. QS values ranging from 0.76 to 2.4 mm s^{-1} are characteristic for μ-oxo dinuclear Fe(III) complexes [1,35,68]. Therefore, the D3 component in FeH-ZSM-5 could be tentatively attributed to two Fe(III) ions each located in the cationic site coordinated to three or four oxygen atoms of the 6MR (containing two Al atoms) and bridged by extra-framework oxygen atom(s) and possibly also to $Fe(III)O^+$ charge balanced by single AlO_4^- species. The D4 component was attributed to Fe(III) species in the close to O_h-like structure of the Fe(III)-oxo oligomers [51]. The broad absorption in the RT experiment (sextuplet at N_2-temperature, Refs. [20,51]), characteristic for large Fe-oxide species, was not observed with FeH-zeolites; see also, absence of absorption in the 12,000–25,000 cm^{-1} region of the Vis spectra (cf. Fig. 5).

The Mössbauer spectra of the steamed evacuated Fe(H)-ZSM-5st zeolites were deconvoluted into five components (D1, D2, D3, D5, D7) (Table 3). The IS and QS parameters of the D1 and D2 components of the steamed zeolites were very similar to those of the FeH-ZSM-5, and thus correspond to the Fe(II) ions in cationic sites. But their intensities substantially decreased from 72% to ~15% for Fe(H)-ZSM-5st. The parameters of the D3 component, assigned to the Fe(III)-oxo species with each located in a cationic site, changed only slightly (IS = 0.35–0.36 mm s^{-1} and QS = 1.94–1.98 mm s^{-1}) as did their intensities. While the D4 component of the Fe(III) oligomers with O_h-like structure was found in the non-steamed zeolites, two new components (D5 and D7) of the Fe(III) species were characteristic for the steamed zeolites. The D5 component (IS = 0.33 mm s^{-1} and QS = 1.38 or 1.42 mm s^{-1}) suggested the presence of Fe(III) in a distorted T_d coordination, as proposed by Lazar et al. [69], but Panov et al. assigned it to Fe(III) oligomers [1]. Nevertheless, the IS and QS values of the D5 component found in the steamed zeolites indicate lower symmetry of the close-to-T_d-coordinated Fe(III), in contrast to the O_h-coordinated Fe(III) of the D4 component. This large difference in the occurrence of oligomeric Fe(III) species in FeH-zeolites and T_d-coordinated Fe(III)

Table 3

Mössbauer parameters and spectral contribution of Fe species in dehydrated FeH- and steamed Fe(H)-ZSM-5st zeolites.

Zeolite	Component	IS (mm s^{-1})	QS (mm s^{-1})	B_{hf} T	Rel.%	Fe species
FeH-Z1	D1	1.02	2.37		32	Fe(II), Fe(II)—O—Fe(II)
	D2	0.93	0.78		40	Fe(II)
	D3	0.31	1.96		19	$[Fe(III)O]^+$, Fe(III)—O_n—Fe(III)
	D4	0.47	2.16		9	Fe(III) oligomers, O_h
FeH-Z2	D1	1.02	2.35		31	Fe(II), Fe(II)—O—Fe(II)
	D2	0.92	0.78		41	Fe(II)
	D3	0.31	2.06		16	$[Fe(III)O]^+$, Fe(III)—O_n—Fe(III)
	D4	0.47	2.16		12	Fe(III) oligomers, O_h
Fe(H)-Z1st	D1	1.21	2.27		7	Fe(II), Fe(II)—O—Fe(II)
	D2	0.98	0.74		8	Fe(II)
	D3	0.36	1.94		8	$[Fe(III)O]^+$, Fe(III)—O_n—Fe(III)
	D5	0.33	1.38		47	Fe(III) in extra-framework Fe—Al—Si, T_d
	D7	0.50		41	30	Fe-oxide species
Fe(H)-Z2st	D1	1.06	2.17		11	Fe(II), Fe(II)—O—Fe(II)
	D2	0.98	0.80		5	Fe(II)
	D3	0.35	1.98		8	$[Fe(III)O]^+$, Fe(III)—O_n—Fe(III)
	D5	0.33	1.42		43	Fe(III) in extra-framework Fe—Al—Si, T_d
	D7	0.50		40	33	Fe-oxide species

ions in the steamed zeolites reflects not only a dramatic reorganization of the Fe(II) ions in cationic sites (a decrease in the concentration of the Fe(II) species), but also a decrease in the oligomeric Fe(III) structures and formation of a new type of T_d-coordinated Fe(III) in Fe—Al—Si extra-framework species. The intensity of the D5 component of the Fe(III) T_d species was estimated to be nearly half of the total iron in Fe(H)-ZSM-5st. The broad background (poorly resolved sextet) reflecting magnetic D7 component (IS 0.50 mm s^{-1} and B_{fh} 40 and 41 T) could originate from the interaction of paramagnetic Fe(III) species. It can be attributed to small Fe-oxide particles, not to isolated Fe(III) oxo complexes or small oligomers bound via cationic sites [1,62,70,71]. Thus, while Fe-oxide particles were not present in FeH-ZSM-5, they represented about one third of the total Fe in the steamed zeolites. Both the T_d-coordinated Fe(III) species (D5 component) and the Fe-oxide-like species in the steamed zeolites appeared predominantly at the expense of the bare Fe(II) ions in cationic sites and oligomeric Fe(III) O_h species, while the dinuclear Fe(III)—O_n—Fe(III) species were less affected (from 19% to 8% and 16% to 8% for Fe-Z1 and Fe-Z2, respectively). Of particular interest is the massive formation of close-to-T_d-Fe(III) ions in Fe—Al—Si extra-framework species and Fe-oxide-like particles in the both steamed Fe(H)-ZSM-5st zeolites, not present in FeH-ZSM-5. Thus substantial changes were observed in the state and coordination of the Fe ions after the zeolite steaming by semi-quantitative analysis of the Mössbauer spectra.

In order to analyze the redox behavior of Fe centers, the Mössbauer spectra of FeH-Z1 and Fe(H)-Z1st samples after their interaction with O_2 at 450 °C, with N_2O at 400 °C, and propane/N_2O (1:1) at 400 °C (followed by evacuation at 400 °C in all cases) were recorded (Fig. 4). Although we had in mind a rough approximation of the coordination of Fe(II) and Fe(III) ions obtained from the spectral parameters, these experiments attempted to simulate the state of Fe species under conditions close to those for N_2O decomposition and propane oxidation. The individual Fe species in both the non-steamed and steamed zeolites exhibited a similar type of reactivity toward O_2, N_2O and propane/N_2O, but the population of the individual Fe products was different (see Tables 4 and 5). The evacuated FeH-ZSM-5 zeolites mostly contained Fe(II) species and only part of the Fe(II) ions in the cationic sites was oxidized by molecular oxygen; roughly, 20% of the Fe(II) ions was oxidized (72–56%) to Fe(III)—O_n—Fe(III) and oligomeric Fe-oxo species. The oxidation of the bare Fe(II) ions in cationic sites was already induced by N_2O at 200 °C (nearly, complete oxidation of the Fe(II) ions was attained at 400 °C). New D6 and D7 components appeared, but practically, none of the Fe(III)—O_n—Fe(III) in the cationic sites (D3 component) were affected, and only a slight increase in the concentration of oligomeric Fe(III)-oxo species (D4) was observed. The parameters of the D6 component with IS = 0.38 and 0.32 mm s^{-1} and QS = 1.09 and 0.94 mm s^{-1} (for the non- and steamed Fe-zeolites, respectively, see Tables 4 and 5), are close to those assigned by Dubkov et al. [1] to Fe(III)—O^- species bearing highly active oxygen. The D7 component represents the magnetic features reflecting the mutually interacting Fe(III)—O^- species [35,50,52]. The relaxation feature appears due to spin–spin interactions within the Fe(III)—O^- complex. In total, 75% of the Fe(III)—O^- species (D6 + D7 components) were formed in FeH-zeolites.

After FeH-Z1 interaction with propane/N_2O at 400 °C, the Fe species mostly exhibited a divalent state (Fig. 4A and Table 4). D1 and D2 components predominated, especially in Fe(II)—O—Fe(II) species. Thus, the propane/N_2O mixture represents a reducing atmosphere for Fe species, and only a small amount of Fe(III) was present. The fitting procedure showed the presence of Fe(III) ions in cationic sites but, as the oligomeric O_h Fe(III) possess close IS and QS parameters, we can hardly quantify these Fe(III) species at low concentrations. It should be pointed out that no D6 component of Fe(III)—O^- was observed. An additional new D8 component

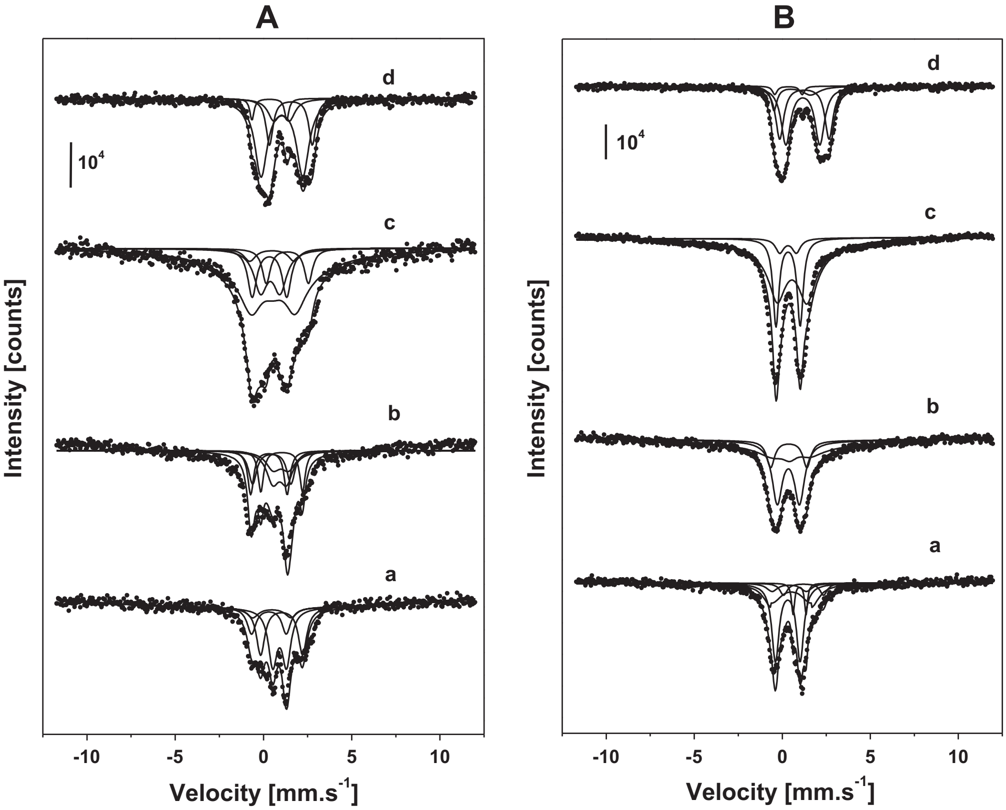

Fig. 4. Mössbauer spectra of (A) FeH-Z1 and (B) steamed Fe(H)-Z1st (a) evacuated at 450 °C, followed by (b) O_2 at 450 °C, (c) N_2O at 400 °C and (d) N_2O/propane (1:1) at 400 °C.

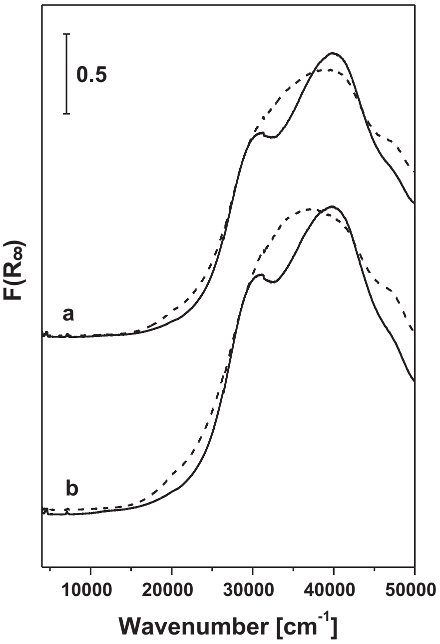

Fig. 5. Comparison of UV–Vis–NIR diffuse reflectance spectra of FeH-ZSM-5 (—) and steamed Fe(H)-ZSM-5st (---) evacuated at 450 °C. (a) FeH-Z1 vs. Fe(H)-Z1st and (b) FeH-Z2 vs. Fe(H)-Z2st.

(IS = 1.50 mm s^{-1}, QS = 2.40 mm s^{-1}) appearing after the propane/N_2O interaction clearly showed divalent Fe(II) T_d-coordinated species [72]. We would not like to speculate on the type of these species, as they might also represent the Fe(II)-ligand complexes originating from the reactants. Further study is needed in this respect.

All these Mössbauer features in the oxidation of Fe-zeolites were also observed for the steamed ones (Fig. 4B and Table 5), but in different proportions. After evacuation, Fe(H)-Z1st contained a much lower concentration (15%) of bare Fe(II) ions in the cationic sites (D1, D2) and already contained Fe-oxide species exhibiting a magnetic component. Most of the bare Fe(II) ions in the cationic sites were oxidized by dioxygen into Fe(III)—O_n—Fe(III) and Fe-oxides. The interaction of the Fe(II) ions with N_2O at a lower temperature (200 °C) did not yield the D5 component of the Fe(III)—O^- species, and these species appeared only at a higher temperature (400 °C) of interaction. Although the Fe(III)—O^- species yield characteristic IS and QS parameters (D6 and D7 components), their quantitative analysis could not be performed for the steamed zeolites, as the magnetic component reflects not only the Fe(III)—O^- species, but also other, not well-defined Fe-oxides present.

Simulation of the *in situ* conditions of propane/N_2O reaction at 400 °C over the steamed Fe(H)-Z1st zeolite showed a predominant concentration of Fe(II) ions (55%) in Mössbauer analysis, close to the D1 component of the Fe(II)—O—Fe(II) species, although the evacuated steamed zeolite contained only 15% Fe(II) in the cationic sites (see Tables 3 and 5). This finding together with a substantial decrease in the concentration of T_d-coordinated Fe(III) and diminishing of Fe(III)—O_n—Fe(III) in the cationic sites indicates that the latter two species were reduced to Fe(II) and appeared as a D8 component in the spectrum. It is to be noted that even Fe-oxide type species were mostly reduced in propane/N_2O at 400 °C as no significant intensity of D7 component was observed.

3.4. UV–Vis–NIR spectra

Fig. 5 compares the UV–Vis–NIR spectra of the FeH-ZSM-5 and steamed Fe(H)-ZSM5st zeolites evacuated at 450 °C. Both FeH-ZSM-5 samples exhibited an intense broad absorption starting from approximately 28,000 cm^{-1} with maximum around 40,000 cm^{-1} with a distinct shoulder at approximately 47,000 cm^{-1}, and well-resolved absorption at 30,500 cm^{-1}. The band at 30,500 cm^{-1} is observed for the hydrated FeH-ZSM-5 at 28,000 cm^{-1} and has previously been ascribed to dinuclear Fe-oxo complexes [73]. However, Pirngruber et al. [26] suggested that it reflects larger Fe-oxo species as followed from the magnetic susceptibility measurements of hydrated Fe-zeolites. As shown by Mössbauer spectral analysis (Section 3.3), the evacuated FeH-ZSM-5 zeolites contained a predominant concentration of Fe(II) and also Fe(III) species. The d–d transitions of the Fe(III) ions are symmetry- and spin-forbidden [74], and the d–d transitions of Fe(II) ions exhibit very weak transitions between 7000 and 10,000 cm^{-1}, reported only at high Fe concentrations in A-type zeolites [75]. Albeit the spectral monitoring was performed here with high sensitivity, we did not observe absorptions corresponding to the d–d transitions of the Fe(II) ions. The observed intense absorption bands of FeH-ZSM-5 could generally reflect O → Fe(III) ligand to metal charge-transfer transitions originating from both extra-framework oxygen and framework oxygen atoms, although a contribution of O→Fe(II) LMCT cannot be excluded.

High-energy absorptions of Fe ions above 33,000 cm^{-1} have been attributed to isolated Fe(III) ions with a frequency reflecting their coordination as analyzed in Fe(III) isomorphously substituted in silicalite [76]. The absorptions at 33,000–50,000 cm^{-1}, attributed to isolated Fe(III) [76], could reflect Fe(III)O^+ species in FeH-ZSM-5, but not bare Fe(III) ions (see the Discussion part). The absorptions below 33,000 cm^{-1} have been assigned to polynuclear Fe-oxo complexes and those below 25,000 cm^{-1} to Fe-oxide-like particles [76]. The shift in the energy of the O → Fe(III) CT transition to lower values might reflect an increasing number of Fe—O bonds in the di- and polynuclear Fe-oxo species like for that of the WO_x clusters [77,78]. A clear absorption maximum at 30,500 cm^{-1} could thus be connected with the dinuclear Fe(III)—O_n—Fe(III) complex or another defined polynuclear Fe(III)-oxo complex, accompanied by the presence of polynuclear Fe-oxo species reflected in lower energy of absorption [26,73,79]. A minimum absorption intensity observed below 25,000 cm^{-1} [79] as well as the absence of the energy edge of bulk-like Fe_2O_3 (occurring at 18,500 cm^{-1} [73]) indicate the absence of larger particles of Fe-oxide in any of the FeH-ZSM-5 zeolites. It should be mentioned that the bare Fe(II) ions in the cationic sites predominating in FeH-ZSM-5 might also exhibit a CT O → Fe(II) transition from the framework oxygen atoms, as observed for divalent bare Co(II) cations [59]. Moreover, some of the O → Fe(III)/Fe(II) CT transitions can occur outside the range of the UV–Vis spectrometers. Therefore, it is concluded that all these uncertainties in the attribution of the UV–Vis spectra to the individual Fe ion species in zeolites, and the lack of knowledge of the extinction coefficients of the CT absorptions prevents their complete analysis.

In agreement with the results of Mössbauer spectroscopy, the steaming of both FeH-zeolites was accompanied by changes in the state of the Fe ions reflected in broadening of the CT absorption of the Fe(III) ions. A significant increase in the intensity around 33,000 and 47,000 cm^{-1} and in the 18,000–25,000 cm^{-1} region was accompanied by an intensity decrease around 40,000 cm^{-1}, while the absorption intensity around 30,500 cm^{-1} was not greatly changed. These findings reflect substantial reorganization of the Fe species during zeolite steaming, particularly the formation of oligomeric entities and small Fe-oxide-like species (from approximately 28,000 cm^{-1} down to 15,000 cm^{-1}) and T_d-coordinated Fe(III) species (absorptions around 47,000 cm^{-1}). The changes in the UV–Vis spectra of Fe(III) species under zeolite steaming are related to a release of framework aluminum into extra-framework sites, reflected in the decreased intensity of the IR vibration of

Table 4
Mössbauer parameters and spectral contribution of Fe species in dehydrated FeH-Z1 and after interaction with O_2, N_2O and C_3H_8/N_2O.

Treatment FeH-Z1	Component	IS (mm s^{-1})	QS (mm s^{-1})	B_{fh} T	Rel. %	Fe species
Evacuated at 450 °C	D1	1.02	2.37		32	Fe(II), Fe(II)—O—Fe(II)
	D2	0.93	0.78		40	Fe(II)
	D3	0.31	1.96		19	$[Fe(III)O]^+$, Fe(III)—O_n—Fe(III)
	D4	0.47	2.16		9	Fe(III) oligomers, O_h
+O_2 at 450 °C	D1	1.02	2.23		15	Fe(II), Fe(II)—O—Fe(II)
	D2	0.93	0.74		41	Fe(II)
	D3	0.31	2.16		28	$[Fe(III)O]^+$, Fe(III)—O_n—Fe(III)
	D4	0.47	2.15		16	Fe(III) oligomers, O_h
+N_2O at 400 °C	D1	1.25	2.38		8	Fe(II), Fe(II)—O—Fe(II)
	D3	0.34	1.95		10	$[Fe(III)O]^+$, Fe(III)—O_n—Fe(III)
	D4	0.48	2.51		7	Fe(III) oligomers, O_h
	D6	0.38	1.09		16	Fe(III)—O^-
	D7	0.5		41	59	Fe(III) relax. component (Fe(III)—O^-)
+C_3H_8/N_2O at 400 °C	D1	1.02	2.37		59	Fe(II), Fe(II)—O—Fe(II)
	D2	0.99	0.79		14	Fe(II)
	D3	0.31	1.96		6	$[Fe(III)O]^+$, Fe(III)—O_n—Fe(III)
	D8	1.50	2.40		21	Fe(II), O_h

the OH groups and C≡N vibrations interacting with the Brønsted sites (see Fig. 1).

The above results of H_2-TPR, FTIR, Mössbauer and UV–Vis spectroscopy reflected substantial changes in the character and concentration of the acid sites and Fe species after steaming of FeH-zeolites under oxidizing conditions. Thus, two quite different couples of samples (i) FeH-ZSM-5 with predominant concentration of Fe(II) and less Fe(III) ions in the cationic sites and containing strongly acidic structural OH groups, and (ii) the steamed Fe(H)-ZSM-5st zeolites with low concentration of acidic protons, low concentration of Fe(II) in cationic sites and high population of T_d-coordinated Fe(III) ions in the Fe—Al—Si extra-framework species and small Fe-oxide particles have been obtained for investigation into their behavior in reactions of nitrous oxide (for summary see Fig. 7). All these specific features of Fe counter-ion species related to changes in the structure and population of the Fe species, their redox behavior, and population of acid sites during Fe-zeolite steaming were observed for both FeH-ZSM-5 samples regardless of the crystal size.

3.5. Nitrous oxide decomposition

Conversion of N_2O to molecular elements and the turn-over-frequency values per total Fe (TOF s^{-1}) at 400 and 425 °C over FeH-ZSM-5 and Fe(H)-ZSM-5st are given in Table 6. The TOF were slightly lower for the nano-crystallites of FeH-Z1 sample exhibiting larger portion of Al-Lewis sites, indicating slightly less developed crystals (see Table 1) compared to FeH-Z2. A marked (ca three-times) decrease in TOF at both temperatures was observed after the steaming of both FeH-zeolites showing partial elimination of Fe active sites for N_2O decomposition.

3.6. Oxidative dehydrogenation of propane to propene with N_2O

Compared to N_2O decomposition, the behavior of the non-steamed and steamed Fe-zeolites in propane/N_2O reaction was more complex and reflected crystal size and changes occurring under steaming with respect to acid sites. Fig. 6 depicts progressive changes with TOS in the propane conversion, yield of propene and CO/CO_2 (CO_x), and the ratio of converted N_2O/C_3H_8 at 400 °C over the FeH-ZSM-5 and Fe(H)-ZSM-5st zeolites. The corresponding TOF per Fe with respect to the converted propane and formed propene and CO_x for TOS of 5, 120, and 240 min are given in Table 7. The initial (at TOS 5 min) TOF_{C3H8} of both FeH-ZSM-5 zeolites, regardless of the crystal size, were similar and exhibited similar decrease with TOS. These initial values were also not significantly affected by the steaming of both zeolites, although the structure of Fe species was markedly changed as reported in Sections 3.1–3.4. But the TOF_{C3H8} and propane conversion (Fig. 6A) over FeH-ZSM-5 decreased with TOS much more compared to the steamed zeolites. On contrary, the initial propene yields (and TOF_{C3H6}) were substantially higher for the steamed zeolites compared to non-steamed ones, and moreover, much more stable values with TOS were found. This finding might indicate much lower propene oligomerization/aromatization and oxidation of these side products as a result of much lower concentration of Brønsted sites (decreased of ca 80%, see Table 2) in the steamed zeolites. The development of the selectivity of propane oxidation over FeH-zeolites with TOS was namely found with larger crystals (2 vs. 0.15 μm); see Fig. 6C and D. The initial ratio of consumed N_2O to propane was close to 2 for long TOS, but it together with the yield of CO_x much more raised up, moreover at shorter TOS for FeH-Z2 (2 μm, 60 min) compared to FeH-Z1 (0.15 μm, 180 min). Contrary to these observations, such development of converted N_2O/propane ratio and CO_x yield with TOS up to 240 min was not observed with both the steamed Fe(H)-zeolites, where the yield of propene only slightly decreased.

These results imply enhanced oligomerization of the formed propene over both non-steamed zeolites owing to high concentration of acidic particularly Brønsted sites and accumulation of more reactive polyolefins and various oxygenates in TOS namely inside the pores of larger (2 μm) crystals of FeH-Z2. As for low concentration of Lewis sites present, their contribution to oligomerization processes cannot be excluded [80]. Beside propene oligomerization, hydrogen transfer reactions leading to paraffins, cyclo-olefins and aromatics, up to coke-like polyaromatic compounds occurs. All these reactions lead to partial blocking of zeolite pore and increasing residence time of reaction products supporting non-selective oxidation.

The concentration and character of the accumulated hydrocarbon products in the pores of FeH- and Fe(H)-ZSM-5st zeolites after TOS of 240 min was estimated by the TPO of the spent catalyst (Table 8). Two distinct maxima of the temperature of release of CO_x (sum of CO and CO_2) at about 470 and 525 °C indicated two major families of deposits, low temperature (LTC) and high-temperature "coke" (HTC). The HTC could be mainly associated with

Table 5
Mössbauer parameters and spectral contribution of Fe species in dehydrated Fe(H)-Z1st and after interaction with O_2, N_2O and C_3H_8/N_2O.

Treatment Fe(H)-Z1st	Component	IS (mm s^{-1})	QS (mm s^{-1})	B_{fh} T	Rel.%	Fe species
Evacuated at 450 °C	D1	1.21	2.27		7	Fe(II), Fe(II)—O—Fe(II)
	D2	0.98	0.74		8	Fe(II)
	D3	0.36	1.94		8	$[Fe(III)O]^+$, Fe(III)—O_n—Fe(III)
	D5	0.33	1.38		47	Fe(III) in extra-framework Fe—Al—Si, T_d
	D7	0.5		41	30	Fe(III) oxide type species
+O_2 at 450 °C	D3	0.37	2.06		13	$[Fe(III)O]^+$, Fe(III)—O_n—Fe(III)
	D5	0.33	1.45		47	Fe(III) in extra-framework Fe—Al—Si, T_d
	D7	0.5		40	40	Fe(III) oxide type species
+N_2O at 400 °C	D5	0.33	1.38		27	Fe(III) in extra-framework Fe—Al—Si, T_d
	D6	0.32	0.94		6	Fe(III)—O^-
	D7	0.5		41	67	Fe(III) relax. component (Fe(III)—O^-, Fe(III) oxide type species)
+C_3H_8/N_2O at 400 °C	D1	1.11	1.99		55	Fe(II), Fe(II)—O—Fe(II)
	D5	0.30	1.33		12	Fe(III) in extra-framework Fe—Al—Si, T_d
	D8	1.16	2.76		33	Fe(II), O_h

poly-condensed aromatic hydrocarbons, while LTC could represent more reactive polyolefins or some oxygenates, oxidized at lower temperatures [81–83]. The total amount of deposits was substantially lower (2–3 times) for the steamed Fe-zeolites (even at a comparable amount of converted propane) containing a higher portion of "olefinic" and "oxygenate" coke (LTC) in comparison with the non-steamed zeolites, where aromatic coke (HTC) predominated.

It can be summarized that the role of the structure of Fe species is not dominant for propane to propene oxidation, while the presence of acid sites and longer contact time in the pores of larger crystals support oligomerization/aromatization of propene formed. The accumulated polyolefinic hydrocarbons in the pores are also readily oxidized finally to CO_x by nitrous oxide and decrease the selectivity to and propene yield (Fig. 6).

4. Discussion

4.1. Structure of Fe species in FeH-ZSM-5

As the counter Fe species in [Al]-substituted zeolites systematically exhibit much higher activity in reactions of N_2O compared to well-dispersed oligomeric and Fe-oxide species supported on silica or silicalite as well as to extra-framework Fe originating from [Fe]-substituted zeolites [31,33], the high N_2O oxidation activity has to be connected with the counter Fe ion species balanced by the negative charge of the framework AlO_4^- tetrahedra. While in metal oxides and aqueous metal salt solutions, the trivalent state of Fe ions is thermodynamically preferred to a divalent one, the negative charge of framework AlO_4^- tetrahedra greatly stabilizes the Fe(II) ions. High TOF values of oxidation of benzene to phenol [3] and propane to propene by N_2O [33] at low Fe concentration indicate that the most active sites are well-dispersed Fe ions, probably Fe(II) in cationic sites.

The interaction of H-zeolites with $FeCl_3$ followed by hydrolysis, with formation of a wide range of hydrolytic products, and calcination [42,84] can lead to the formation of various Fe species, such as bare Fe(II) ions, monomeric, dimeric, and oligomeric Fe(III)-oxo species, and small Fe-oxide-like species up to bulk Fe-oxides. The populations of these species depend on the degree and conditions of Fe incorporation on the one hand, and the AlO_4^- distribution in the parent zeolite framework governing the local negative charge at the framework rings, on the other hand. In general, the Al atoms in the ZSM-5 framework are predominantly (>95%) distributed among (i) Al—O—(Si—O)$_2$—Al sequences in the framework rings of cationic sites (denoted as Al pairs) and (ii) distant single Al atoms occurring in different rings (Al—O—(Si—O)$_{n>2}$—Al sequences). The distribution of Al atoms in high-silica zeolites is discussed in details in Ref. [66]. Although we did not investigate here the effect of the distribution of framework Al atoms in the presented zeolites on the structure of the incorporated Fe species, the existing local negative charge should be considered to affect the structure of the stabilized counter Fe ion species. At the low Fe loadings of FeH-ZSM-5 (Fe/Al 0.15) reported here, the Fe species are represented by counter-ion Fe species, predominantly by bare Fe(II) ions, as also reported in Refs. [34,35,42,68,85], necessarily charge balanced by Al pairs in the framework rings of cationic sites (72% for both FeH-Z1 and FeH-Z2). As the ZSM-5 zeolites of Si/Al > 12 do not contain Al—O—Si—O—Al sequences in their framework, as obtained by ^{29}Si MAS NMR analysis (see Refs. [66,86]), the absence of the latter Si—Al sequences implies the absence of three Al atoms in the 6MRs of the cationic sites, and thus the inability of ZSM-5 to coordinate bare Fe(III) ions. The Fe(III)-oxo species represent a lower fraction in dehydrated auto-reduced zeolites (see Table 3), where Fe ions of dimeric Fe(III)—O_n—Fe(III) are balanced either by two Al pairs or presumably in oligomeric Fe(III)-oxo species by single Al atoms. The bonding of Fe ion species in cationic sites also follows from a decrease in the concentration of the structural SiOHAl groups of FeH-ZSM-5 compared to the parent zeolites (Fig. 1A and Table 2). The presence of bare Fe(II) ions was demonstrated by their interaction with the C≡N group of adsorbed d_3-acetonitrile, yielding a vibration frequency at 2303 cm^{-1} (Fig. 1B and Table 2). The Fe(II)/Fe(III) distribution in FeH-ZSM-5 is sensitive to the conditions of the zeolite treatment. While FeH-zeolites evacuated at 450 °C resulted predominantly in Fe(II) species (72% Fe(II); see Fig. 4 and Tables 3 and 4), only a small fraction of Fe(II) in FeH-ZSM-5 is oxidized by molecular oxygen at 450 °C to Fe(III). This shows high stabilization of the bare Fe(II) ions by framework rings of the cationic sites containing two Al atoms (Al pairs) as reflected in the D2 component of the Mössbauer spectra (Table 3). The dinuclear Fe(II)—O—Fe(II) species (D1 component in Table 3) might represent Fe ions each coordinated to a framework ring containing a single Al atom.

A possible model solution for the isolated Fe(III) ion would be coordination of the OH^- ligand with a total complex charge of (2+), as suggested, for example, in Refs. [42,87]. But such hydroxyls dehydroxylate above 350 °C with participation of skeletal protons and are converted to Fe(II) ions. Fe(II) ions balanced by an Al pair in the framework 6MR have a highly stabilized valence, not reduced to metallic Fe and with difficulty oxidized to Fe(III). Accordingly, the hydroxy $[Fe(III)OH]^{2+}$ species, if charge balanced by two AlO_4^-, can be either transformed to bare Fe(II) ions in cationic sites or might form dinuclear Fe(III)—O_n—Fe(III) complexes with each of the Fe(III) ions coordinated in the cationic site. Another possible

Table 6
Decomposition of N_2O over FeH-ZSM-5 and steamed Fe(H)-ZSM-5st. Conditions: 1000 ppm N_2O in He, catalyst 50 mg, GHSV 180,000 h^{-1}.

Zeolite	Conversion (%)		TOF × 10^4 (s^{-1})	
	400 °C	425 °C	400 °C	425 °C
FeH-Z1	2.0	4.2	7.2	15
Fe(H)-Z1st	0.6	1.9	2.2	6.9
FeH-Z2	2.2	4.7	9.3	19
Fe(H)-Z2st	0.7	1.5	3.0	6.4

hydroxylated Fe(III) species could be assumed the $[Fe(III)(OH)_2]^+$ complex charge balanced by a single AlO_4^-, which might be transformed after dehydration into isolated $Fe(III)O^+$. However, we have no straightforward spectral evidence for the presence of these complexes, which might be reflected in the UV–Vis spectra in the region from 33,000 to 50,000 cm^{-1}. It is concluded that the single Fe(II) ions and various Fe(III)-oxo and Fe(II)/Fe(III)-oxo oligomeric entities can, in principle, be formed from the above Fe-hydroxylated complexes, and charge balanced by framework AlO_4^- entities:

$$\begin{array}{lll}
[Fe(III)OH^-]^{2+}\cdots 2AlO_4^- & \rightarrow & Fe(II)\cdots 2AlO_4^- \\
 & \rightarrow & 2AlO_4^-\cdots Fe(III){-}O{-}Fe(III)\cdots 2AlO_4^- \\
[Fe(III)(OH^-)_2]^+\cdots AlO_4^- & \rightarrow & [Fe(III)O]^+\cdots AlO_4^- \\
 & \rightarrow & AlO_4^-\cdots Fe(II){-}O{-}Fe(III)\cdots 2AlO_4^- \\
[Fe(II)(OH)]^+\cdots AlO_4^- & \rightarrow & AlO_4^-\cdots Fe(II){-}O{-}Fe(II)\cdots AlO_4^-
\end{array}$$

For illustration of the population of the individual Fe species, see Fig. 7.

The formation of dinuclear Fe(II) or Fe(III) complexes bridged by one or two oxygen atoms also depends on the distances between the respective Fe ions and extra-framework oxygen atoms acceptable for the formation of the Fe—O bond. The dinuclear Fe(III)-oxo complexes consisting of Fe(III) or Fe(II)/Fe(III) ions have been found specifically at higher Fe loadings [2,20,88]. At Fe loadings (Fe/Al ~ 1) mostly prepared by $FeCl_3$ sublimation, the presence of dinuclear Fe-oxo complexes was clearly indicated by XANES, EXAFS [43] and magnetic susceptibility measurements [26], but their quantitative analysis is not unambiguous [26].

Oxidation of FeH-ZSM-5 by N_2O transforms Fe(II) to the $Fe(III){-}O^-$ entities with the characteristic D6 (IS = 0.38 mm s^{-1} and QS = 1.09 mm s^{-1}) and broad D7 magnetic relaxation components, reflecting spin–spin interactions of the d^1 and s^1 electrons within the $Fe(III){-}O^-$ complex (Fig. 4, Tables 4 and 5). A suggestion on the radical character of the α-oxygen bound to the Fe(III) ions given by Panov [1,9,89] is supported by its high reactivity, but no direct experimental evidence has been reported. It should be stressed that the concentration of the formed $Fe(III){-}O^-$ species depends on the state of the Fe ions. Divalent Fe ions with an open coordination sphere are candidates for binding oxygen atoms from N_2O. The temperature of Fe-zeolite evacuation [27,29] and temperature and composition of $NO_x/C_xH_y/O_2$ and $NO_x/NH_3/O_2$ reactant mixtures [30,53,90,91] or propane/N_2O reported here (Tables 4 and 5), are shown to highly affect the concentration of Fe(III)/Fe(II) ions.

The estimation of the population of $Fe(III){-}O^-$ and Fe(III)-oxo species based on the individual IS and QS parameters of the Mössbauer spectra (Tables 4 and 5) is supported by the H_2-TPR of FeH-ZSM-5 (Figs. 2 and 3). While the $Fe(III){-}O_n{-}Fe(III)$ and oligomeric Fe(III)-oxo species are reduced at higher temperatures in a broad temperature range from 300 to 500 °C, the N_2O already at 200 °C produces a sharp peak at 230 °C in the TPR, reflecting reduction in $Fe(III){-}O^-$ species. This very reactive $Fe(III){-}O^-$ species [34], increases in concentration with increasing temperature of the N_2O interaction up to 400 °C (Fig. 2), implying existence of Fe(II) species of various reactivity with respect to N_2O. The $Fe(III){-}O^-$ entities formed from Fe(II) in the cationic sites, corresponding to Panov's α-sites [1], have been suggested as the most active sites for hydroxylation of hydrocarbons. The high reactivity of the $Fe(III){-}O^-$ entities and presence of a spectrum of Fe species of various reducibility is also demonstrated by the interaction of C_3H_8/N_2O (1:1) at 400 °C with FeH-Z1 yielding only bare and bridged Fe(II) ions, oligomeric Fe(II), while only low concentration of counter Fe(III)-oxo complexes was preserved (Table 4).

The broad UV absorption with a maximum at about 40,000 cm^{-1}, shoulder at 47,000 cm^{-1} and the distinct absorption at 30,500 cm^{-1} could reflect the CT transition of $Fe(III)O^+$, various dinuclear $Fe(III){-}O_n{-}Fe(III)$ and small polynuclear Fe-oxo species, while those down to 25,000 cm^{-1} (Fig. 5) represent oligomeric Fe-oxo species, as also manifested in H_2-TPR. While $Fe(III)O^+$ and dinuclear $Fe(III){-}O_n{-}Fe(III)$ entities are reduced from ca 250 to 400 °C, oligomeric Fe-oxo species consumed hydrogen at 400–500 °C (Figs. 2 and 3). The oligomeric Fe-oxo species (D4 component, Table 3) might be connected with the rings containing single Al atoms. The changes in the relative concentrations of the individual Fe(II) and Fe(III) species with the zeolite calcination in dioxygen indicates transformation of part of the Fe(II) ions into Fe(III) ions in the cationic sites and oligomeric Fe-oxo species [26,73,79], while only N_2O yields a very reactive $Fe(III){-}O^-$ entity reflected in the D6 and D7 relaxation component (Table 4). However, the Fe(III)-oxo species themselves, if not previously reduced to Fe(II) ions, could not contribute to the formation of $Fe(III){-}O^-$, as occurs with Fe(II) ions in cationic sites. On the other hand, the Fe(III)-oxo species participates in redox-type reactions of hydrocarbons occurring with molecular oxygen or NO/NO_2 in their selective catalytic reduction by ammonia or hydrocarbons [30,41,42,45,92].

4.2. Effect of the steaming on the acid sites and Fe ion species

It is well known that the steaming of H-zeolites is accompanied by a release of the framework Al atoms into the extra-framework sites, resulting in a substantial decrease in the concentration of bridging OH groups, formation of Al-electron-acceptor sites and alumina or aluminosilicate species in the pores, as observed in parent H-zeolites (Fig. 1 and Table 1). The presence of Fe ions in cationic sites (like any other metal ions) stabilizes the adjacent framework Al atoms [87]. But Al released into the pores mostly from the framework Al atoms balanced by protons interacts with Fe ions in the cationic sites (bare Fe(II) ions) and much less with dinuclear $Fe(II){-}O{-}Fe(II)$ and $Fe(III){-}O_n{-}Fe(III)$ species, as indicated by the Mössbauer spectra (see Table 3). Thus, the steaming results in major reorganization of Fe(II) in the cationic sites as well as oligomeric Fe-oxo species, and in the appearance of a high concentration of T_d-coordinated Fe(III) ions (component D5), accompanied by small Fe-oxide particles (magnetic D7 component, Table 3). It can be speculated that Al atoms released from the framework under steaming in an oxidizing atmosphere form some aluminosilicate species, which encapsulate oxidized Fe(II) ions originally located in cationic sites and Fe(III) oligomeric species. In both steamed Fe-samples (dehydrated under vacuum), about 75% of Fe is in the form of T_d-Fe(III) and small Fe-oxide particles, while Fe(II) ions in cationic sites are low populated (~15%), in contrast to the non-steamed FeH-ZSM-5 containing predominantly Fe(II) ions (72%) as schematically summarized in Fig. 7.

The dramatic reorganization of the bare Fe(II) ions, induced by the release of Al from the framework under steaming, is supported by (i) the shift in the broad band with around 40,000–35,000 cm^{-1}, (ii) its broadening below 25,000 cm^{-1} and the appearance of the energy edge at 18,500 cm^{-1} in the UV–Vis spectra (Fig. 5), thus reflecting an increase in the concentration of oligomeric species

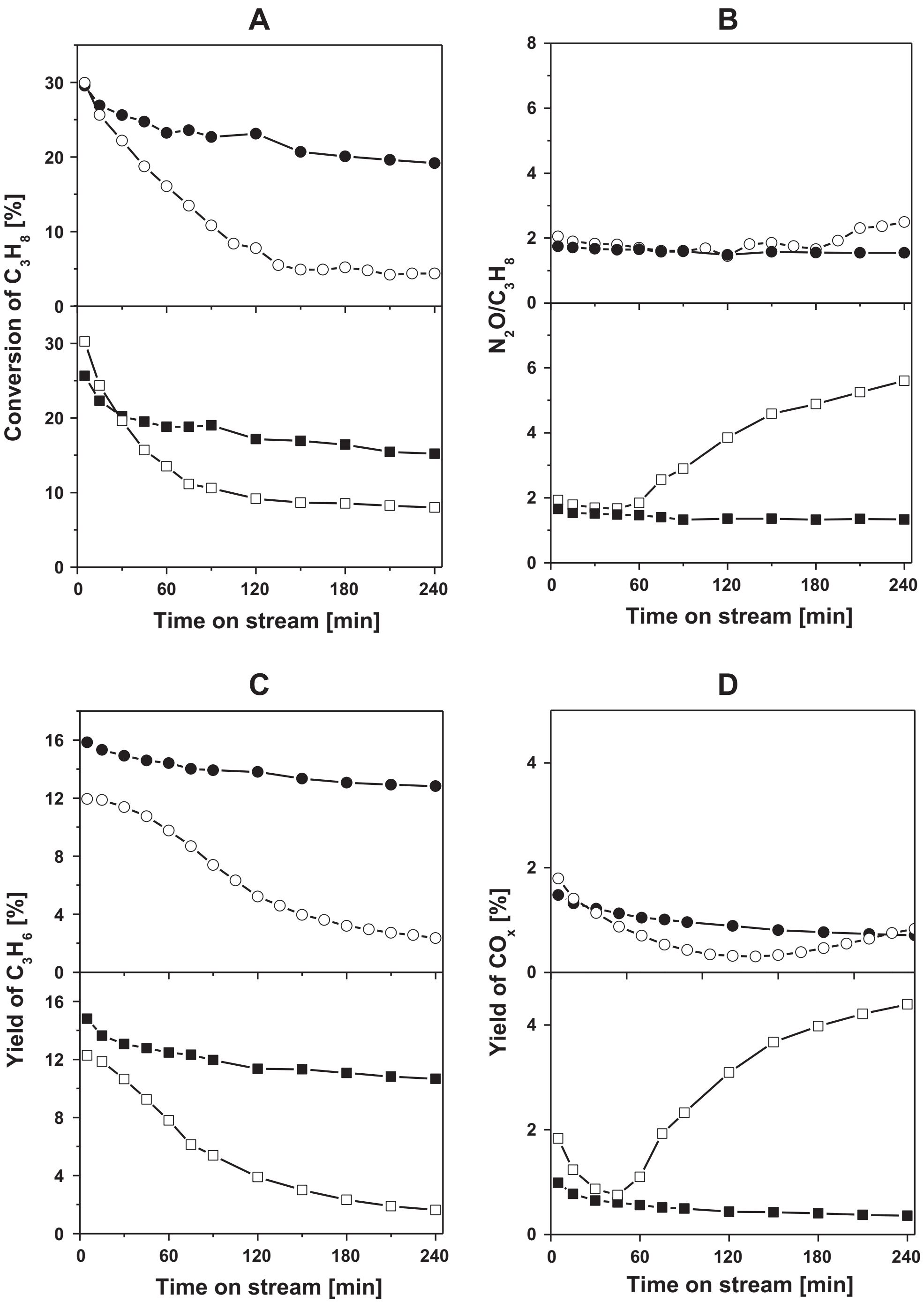

Fig. 6. Oxidation of propane by N_2O over FeH-ZSM-5 and steamed Fe(H)-ZSM-5st. (A) conversion of C_3H_8, (B) ratio of converted N_2O to C_3H_8, and yield of (C) C_3H_6 and (D) CO_x over FeH-Z1 (–○–), Fe(H)-Z1st (–●–), FeH-Z2 (–□–) and Fe(H)-Z2st (–■–). Conditions: 50 mg catalyst, 1.5% N_2O and 1.5% C_3H_8 in He, WHSV 3.5 h^{-1}, T 400 °C.

and formation of Fe-oxide particles, and (iii) the shift in the reduction in Fe(H)-ZSM-5st zeolites by hydrogen to around 460 °C, and almost two-fold increase in hydrogen consumption, characteristic for larger Fe(III)-oligomeric or oxide species (Figs. 2 and 3). These findings indicate clustering of Fe(III)-oxo species to Fe-oxide particles, in agreement with Refs. [61,87,92,93], and binding of Fe(III) species in an alumina or aluminosilicate amorphous particles.

The changes in the valence and structure of Fe complexes invoked by steaming are also reflected in the Fe(II)/Fe(III) transformations under evacuation, and interaction with dioxygen, N_2O and propane/N_2O at the reaction temperature of 400 °C (Table 5 Fig. 4B). All the remaining Fe(II) ions in the steamed Fe(H)-ZSM-5st zeolites were oxidized by oxygen at 450 °C. Practically no Fe(III)—O^- entities were formed at 200 °C under Fe(H)-Z1st interaction with N_2O, and 400 °C was required for the Fe(III)—O^- formation (component D6 and D7 in Table 5), as also indicated by the H_2-TPR results (Figs. 2 and 3). Although quantitative analysis of the Fe(III)—O^- species by Mössbauer spectra in the steamed zeolites was not possible (Table 5 and Fig. 4B), we can conclude that most of the Fe(III) species (~90%) present, that is, the T_d-coordinated Fe(III) associated with the Fe—Al—Si extra-framework species and small Fe-oxide particles, were reduced in a propane/N_2O (1:1) mixture at 400 °C (Table 5). Thus, the steamed Fe-zeolites interacting with N_2O yielded lower concentrations of Fe(III)—O^- compared to

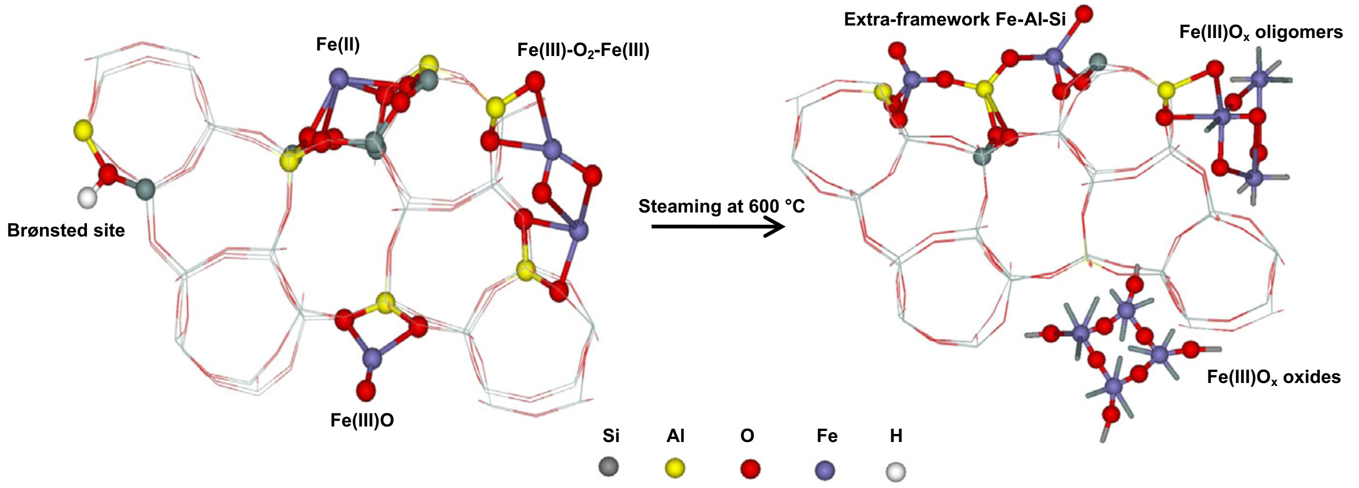

	Non-steamed	Steamed at 600 °C
Fe(II), Fe(II)-O-Fe(II)	**61-72%**	**9-16%**
Fe(III)O, Fe(III)-O$_n$-Fe(III)	**15-19%**	**8-14%**
Fe(III) in extra-framework Fe-Al-Si	**not present**	**43-48%**
Fe(III)O$_x$ oligomers, O$_h$	**9-24%**	**26-33%**
Fe$_2$O$_3$ oxides	**not present**	

	Non-steamed	Steamed at 600 °C
$c_{Brønsted}$ [mmol g^{-1}]	**0.26-0.31**	**0.05**
$c_{Al\text{-}Lewis\ sites}$ [mmol g^{-1}]	**0.04-0.09**	**0.03-0.04**

Fig. 7. Main Fe structures in FeH-ZSM-5 (Fe/Al ~ 0.15, Si/Al ~ 22) and their reorganization under steaming at 600 °C for 4 h. Fe speciation after evacuation at 450 °C for 3 h.

Table 7
Turnover frequency per Fe for propane, propene and CO$_x$ in oxidation of propane by N$_2$O over FeH-ZSM-5 and steamed Fe(H)-ZSM-5st for TOS 5, 120 and 240 min. Conditions: 1.5% N$_2$O and 1.5% C$_3$H$_8$ in He, WHSV 3.5 h^{-1}, T 400 °C.

Zeolite	TOF$_{C3H8}$ × 10^2 (s^{-1})			TOF$_{C3H6}$ × 10^2 (s^{-1})			TOF$_{COx}$ × 10^2 (s^{-1})		
	5 min	120 min	240 min	5 min	120 min	240 min	5 min	120 min	240 min
FeH-Z1	5.4	1.4	0.8	2.2	0.9	0.4	1.0	2.0	2.9
Fe(H)-Z1st	5.3	4.2	3.5	2.9	2.5	2.3	0.8	0.6	0.4
FeH-Z2	6.4	1.9	1.7	2.6	0.8	0.3	1.2	1.5	2.8
Fe(H)-Z2st	5.4	3.6	3.2	3.1	2.4	2.3	0.6	0.3	0.2

Table 8
Coke deposition in spent Fe-ZSM-5 catalysts after C$_3$H$_8$/N$_2$O at 450 °C after TOS 4 h.

Sample	Total ($g_{coke}\ g_{cat}^{-1}$)	LTC[a] ($g_{coke}\ g_{cat}^{-1}$)	HTC[b] ($g_{coke}\ g_{cat}^{-1}$)
FeH-Z1	0.28	0.10	0.18
Fe(H)-Z1st	0.09	0.05	0.04
FeH-Z2	0.17	0.05	0.12
Fe(H)-Z2st	0.09	0.03	0.06

[a] Coke oxidized at 300–500 °C.
[b] Coke oxidized at 500–650 °C.

FeH-ZSM-5, but in the presence of propane gave a comparable degree of reduction in Fe(III) to Fe(II) regardless of the fact that the original Fe species possessed a quite different structure (see Fig. 7). This implies existence of a spectrum of Fe species, which under suitable conditions for their reduction can provide Fe(II) ions with an open coordination sphere available for the interaction with N$_2$O.

4.3. The effect of Fe species and acid sites in FeH- and Fe(H)-ZSM-5st on nitrous oxide decomposition and propane oxidation by N$_2$O

It is assumed that, in the transformation of N$_2$O to molecular products, the formation of α-oxygen of the Fe(III)—O$^-$ complex is very fast, while the rate-determining step is the formation of molecular oxygen by recombination of two α-oxygen atoms or their interaction with an additional N$_2$O molecule [1,37]. Kapteijn et al. [37] reported TOF per Fe equal to 1.7 × 10^{-2} s^{-1} at 400 °C for the reaction of Fe site with N$_2$O, and TOF 2.8 × 10^{-4} s^{-1} for the reaction of Fe(III)—O$^-$ complex with N$_2$O, as obtained from the kinetics analysis. The TOF values per total Fe reported here for N$_2$O decomposition over both FeH-zeolites are higher (7.2 × 10^{-4} and 9.3 × 10^{-4} s^{-1}) indicating that more active or higher portion of the most active Fe sites are present in these zeolites. The finding that the interaction of Fe site with N$_2$O yielding Fe(III)—O$^-$ complex is faster is also proven here by the simulated *in situ* reaction conditions at 400 °C (monitored by Mössbauer analysis at RT). It showed nearly quantitative transformation of Fe(II) ions in the cationic sites of FeH-Z1 into Fe(III)—O$^-$ complexes (75% of Fe ions, see Table 4).

The steaming of FeH-zeolites, dramatically changing the structure of Fe species and resulting in that only approximately 20% of the Fe(II) species originally present (see Table 3), yielded a significant decrease in TOF to ~30% of the original value (to 2.2 × 10^{-4} and 3.0 × 10^{-4} s^{-1}). This finding might also be supported by a lower concentration of isolated Fe(III)—O$^-$ in the steamed Fe-zeolites, as shown by Mössbauer analysis (Table 5; note that the population of Fe(III)—O$^-$ can hardly be determined due to relaxation component) and H$_2$-TPR experiments (Figs. 2 and 3). It is to be mentioned that some contribution of the defective sites [93] or adjacent Al-Lewis sites in the steamed zeolites [94] (very low concentration here) to the recombination of α-oxygen atoms to dioxygen or their reaction with N_2O molecule cannot be excluded.

It can be concluded that a clear and similar decrease in TOF of N_2O decomposition and concentration of Fe(II) in cationic sites from FeH- to steamed Fe(H)-ZSM-5st zeolites (compared on evacuated samples), and an increased population of Fe(III)-oxo species, particularly of T_d-coordinated Fe(III) (Tables 3 and 5) indicate that the most active sites for N_2O decomposition are Fe(II) ions in cationic sites coordinated to framework rings containing an Al pair. The reaction rate is controlled by the reaction step of the Fe(III)—O^- complex with N_2O transformed into molecular components, while the first step, the complex formation is very fast. High TOF values were reached in this study as Fe-zeolites contained prevailing concentration of bare Fe ions in cationic sites.

Conversion of propane with N_2O occurs through its hydroxylation to propanol over an Fe(III)—O^- complex, followed by immediate dehydration to propene (Eq. (4)), which could be further transformed over acid sites to various oligomers, aromatics, and to low hydrocarbons by their cracking, and on redox Fe sites to various oxygenates of polyolefins, and carbon oxides.

The TOS analysis of conversion of propane, yields of propene and CO/CO_2, and relative consumption of N_2O and character of deposits formed compared over FeH- and steamed Fe(H)-zeolites (Fig. 6 and Table 8) showed detrimental effect of the high concentration of Brønsted sites on the propene yield and a decrease in propane conversion. This is owing to oligomerization of propene up to polyaromatics and enhanced oxidation of more reactive polyolefins by N_2O to oxygenates up to CO/CO_2. This is in line with the absence of this behavior in the steamed Fe(H)-zeolites containing a very low concentration of Brønsted acid sites (Table 2). A sharp increase in CO_x yield after 60 min of TOS for FeH-Z2 with larger crystals (without significant changes in propane conversion, see Fig. 6A and C) and simultaneous increase in the ratio of converted N_2O/C_3H_8 in contrast to nano-size FeH-Z1 suggests longer residence time of reactants in the restricted pores and accumulation of highly reactive polyolefins. It implies that beside the presence of active Fe sites, the important conditions for selective oxidative dehydrogenation of propane with N_2O is low concentration of Brønsted sites and small crystallites enabling fast removal of propene from the pores and thus suppressing its oligomerization.

The oxidation of propane by nitrous oxide over the individual Fe species undoubtedly proceeds via the "α-oxygen" of the Fe(III)—O^- complex formed by the interaction of Fe(II) ions with N_2O. Albeit the steamed Fe(H)-ZSM-5st exhibited much lower concentration of bare Fe(II) ions in the cationic sites compared to FeH-ZSM-5 (as analyzed after vacuum or oxygen heat pre-treatment, cf. Tables 3–5), under the "*in situ*" conditions of propane/N_2O/400 °C, about 90% of the Fe species for both FeH- and steamed Fe(H)-Z1 was in a divalent state (Tables 4 and 5). The comparable initial TOF_{C3H8} for non-steamed and steamed Fe-zeolites and the higher TOF_{C3H6} for both steamed zeolites (Table 7), and reduction in the most of Fe ions under reaction condition (Tables 4 and 5) to a divalent state indicates that the concentration of Fe active sites in non- and steamed zeolites was not significantly different. It suggests that, under the C_3H_8/N_2O feed at the more reducing conditions compared to those at N_2O decomposition (see Tables 4 and 5), also the $Fe(III)O^+$ and Fe(III)-oxo species attached to rings with Al pairs or single Al atoms (dinuclear and oligomeric) in FeH-zeolites as well as the T_d-coordinated Fe(III) in the steamed Fe-zeolites connected with the Fe—Al—Si extra-framework species are both reduced to Fe(II) ions. Thereafter these even less reactive divalent Fe species could take part in the formation of Fe(III)—O^- species, especially at temperature of 400 °C.

There remains the question of the structure of the Fe sites active in propane oxidation in the steamed Fe-zeolites, with highly populated T_d-coordinated Fe(III) connected with in the Fe—Al—Si extra-framework species in the steamed zeolites. The high TOF values per Fe observed at very low Fe loadings over Fe-ZSM-5 indicated that the most active sites in benzene oxidation to phenol and propane to propene are atomically dispersed Fe ions [3,31,33,95], but a comparable activity of the non-steamed and steamed Fe-zeolites (substantially differing in the concentration of bare Fe(II) ions in cationic sites) indicates that, in propane/N_2O, other Fe sites also contribute to the reaction. This assumption is supported by the much higher TOF for conversion of N_2O in propane/N_2O to propene (ca 75× for FeH-Z1 and ca 270× for Fe(H)-Z1) compared to N_2O decomposition (cf. Tables 6 and 7). Pirutko et al. [7] also showed that under the same concentration conditions over Fe-ZSM-5, the N_2O decomposition is approximately 100 times slower compared to benzene/N_2O reaction. We assume that the N_2O decomposition requires the presence of Fe(II) ions highly stabilized in the oxidizing atmosphere of this reaction, which is satisfied only by Fe(II) ions in cationic sites balanced by two framework Al atoms. On contrary under the reducing conditions of the propane/N_2O reaction, the Fe species possessing lower reducing potential are also reduced to Fe(II), like Fe(III)-oxo species balanced by single Al atoms and even T_d-coordinated Fe(III) ions bound to the Fe—Al—Si extra-framework species. All these Fe(II) sites form Fe(III)—O^- entities. Presumably, the activity of these Fe(II) species is lower compared to Fe(II) in cationic sites, and they need a temperature of 400 °C for their interaction with N_2O to form highly reactive Fe(III)—O^- (cf. H_2-TPR in Figs. 2 and 3, and Mössbauer analysis results). A significant increase in the yield of selective products over the steamed Fe-zeolites was also reported for benzene to phenol [3,22,96] and propane to propene [95]. Our suggestion on the activity of T_d-coordinated Fe(III) species in propane oxidation in the steamed Fe(H)-zeolites is in agreement with the reports of Hensen et al. [22] and Ates et al. [97], who explained the increased activity of steamed zeolites by the formation of an undefined Fe(III)-oxo species ("Fe—Al—O" species), closely connected with Al present in the steamed zeolites. Nevertheless, beside the contribution of these Fe species to the hydrocarbon oxidation, the concentration of Brønsted sites should be taken seriously into account.

From the above results we conclude that under the conditions of propane/N_2O, majority of Fe species in both FeH- and steamed Fe(H)-ZSM-5 are reduced to Fe(II), while at N_2O decomposition Fe(III)—O^- highly prevail. It can be supposed that the rate-determining step of the propane oxidative dehydrogenation by nitrous oxide is formation of Fe(III)—O^- from Fe(II) and N_2O, contrary to N_2O decomposition, where the reaction is determined by the Fe(III)—O^- recombination or its reaction with additional N_2O molecule. The Fe(III)—O^- complex rapidly reacts with propane to propanol dehydrated to propene. A further non-selective transformation of propene is controlled by the concentration of Brønsted acid sites leading to propene oligomerization, and more reactive oligomers are readily oxidized to various oxygenates and finally to carbon oxides.

5. Conclusion

The critical function of the structure of Fe counter-ion species, Brønsted sites and crystal size of Fe-ZSM-5 for propane oxidative dehydrogenation to propene and N_2O decomposition was elucidated by using two series of Fe-zeolites with crystal size 0.15 and 2 μm differing in population of the individual Fe and Brønsted sites. Firstly, FeH-ZSM-5 with predominant abundance of Fe(II) ions in the cationic sites (72%), a minor part of the ion-exchanged Fe(III)-oxo species (16–19%) and without an excessive formation of oligomeric Fe(III) species (9–12%) and large oxide species were prepared. Steaming of these Fe-zeolites at 600 °C resulted in a low concentration of Fe(II) ions and Fe-oxo species in the cationic sites. Predominant part of Fe was T_d-coordinated Fe(III) (43–47%) bound within extra-framework Fe—Al—Si species, and as Fe-oxide particles (30–33%). It has been shown that the N_2O decomposition over Fe-zeolites is governed by the concentration of Fe(II) balanced by Al pairs in the framework cationic sites. Formation of Fe(III)—O^- by the reaction of Fe(II) with N_2O is very fast and the rate-determining step is the transformation of Fe(III)—O^- to molecular oxygen. Under the reducing conditions of propane/N_2O reaction at 400 °C not only Fe in cationic sites, but also T_d-coordinated Fe(III) in extra-framework Fe—Al—Si were reduced to Fe(II) ions (90% of total Fe) in both the non-steamed and steamed Fe-zeolites.

Beside Fe(II) ions highly stabilized by framework rings with two AlO_4^- charges, also other Fe(III)-oxo species reduced to Fe(II) under the conditions of propane/N_2O reaction provide opportunity to form Fe(III)—O^-, which immediately interacts with propane. The turn-over-frequencies of propane/N_2O reaction were of two orders higher compared to those of N_2O decomposition for both FeH- and steamed Fe(H)-ZSM-5st zeolites. Therefore, the rate-determining step in propane/N_2O is suggested to be formation of Fe(III)—O^- complex, immediately interacting with propane. Beside the Fe(II) sites formed at the reaction conditions protonic sites contribute to the overall process of propane oxidation. The higher and stable yields of propene were achieved over the steamed Fe-zeolites. That was mainly caused by the low concentration of protonic sites limiting propene oligomerization. On contrary, with FeH-ZSM-5 and particularly of larger crystals, retention of more reactive polyolefins in the pores in TOS increases their oxidation to CO/CO_2.

Acknowledgments

This study was supported by The Czech Science Foundation (Projects #P106/11/0624 and 203/09/1627) and by RVO #61388955.

Appendix A. Supplementary material

Supplementary data associated with this article can be found, in the online version, at http://dx.doi.org/10.1016/j.jcat.2012.12.010.

References

[1] K.A. Dubkov, N.S. Ovanesyan, A.A. Shteinman, E.V. Starokon, G.I. Panov, J. Catal. 207 (2002) 341–352.
[2] G.I. Panov, G.A. Sheveleva, A.S. Kharitonov, V.N. Romannikov, L.A. Vostrikova, Appl. Catal. A: Gen. 82 (1992) 31–36.
[3] P. Kubanek, B. Wichterlova, Z. Sobalik, J. Catal. 211 (2002) 109–118.
[4] J.F. Jia, K.S. Pillai, W.M.H. Sachtler, J. Catal. 221 (2004) 119–126.
[5] I. Yuranov, D.A. Bulushev, A. Renken, L. Kiwi-Minsker, J. Catal. 227 (2004) 138–147.
[6] K. Sun, H. Xia, Z. Feng, R. van Santen, E. Hensen, C. Li, J. Catal. 254 (2008) 383–396.
[7] L.V. Pirutko, V.S. Chernyavsky, E.V. Starokon, A.A. Ivanov, A.S. Kharitonov, G.I. Panov, Appl. Catal. B: Environ. 91 (2009) 174–179.
[8] N.S. Ovanesyan, K.A. Dubkov, A.A. Pyalling, A.A. Shteinman, J. Radioanal. Nucl. Chem. 246 (2000) 149–152.
[9] E.V. Starokon, M.V. Parfenov, L.V. Pirutko, S.I. Abornev, G.I. Panov, J. Phys. Chem. C 115 (2011) 2155–2161.
[10] J. Perez-Ramirez, A. Gallardo-Llamas, J. Catal. 223 (2004) 382–388.
[11] R. Bulanek, B. Wichterlova, K. Novoveska, V. Kreibich, Appl. Catal. A: Gen. 264 (2004) 13–22.
[12] E.V. Kondratenko, J. Perez-Ramirez, Appl. Catal. A: Gen. 267 (2004) 181–189.
[13] O. Sanchez-Galofre, Y. Segura, J. Perez-Ramirez, J. Catal. 249 (2007) 123–133.
[14] N.K. Sathu, P. Sazama, V. Valtchev, B. Bernauer, Z. Sobalik, Oxidative dehydrogenation of propane over Fe-BEA catalysts, Stud. Surf. Sci. Catal. (2008) 1127–1130.
[15] L. Kiwi-Minsker, D.A. Bulushev, A. Renken, J. Catal. 219 (2003) 273–285.
[16] J. Novakova, Z. Sobalik, Catal. Lett. 127 (2009) 95–100.
[17] J. Novakova, Z. Sobalik, Catal. Lett. 131 (2009) 530–537.
[18] H. Guesmi, D. Berthomieu, L. Kiwi-Minsker, Catal. Commun. 11 (2010) 1026–1031.
[19] J. Perez-Ramirez, F. Kapteijn, A. Bruckner, J. Catal. 218 (2003) 234–238.
[20] E.J.M. Hensen, Q. Zhu, M.M.R.M. Hendrix, A.R. Overweg, P.J. Kooyman, M.V. Sychev, R.A. Van Santen, J. Catal. 221 (2004) 560–574.
[21] Q. Zhu, R.M. Van Teeffelen, R.A. Van Santen, E.J.M. Hensen, J. Catal. 221 (2004) 560–568.
[22] E. Hensen, Q. Zhu, P.H. Liu, K.J. Chao, R. Van Santen, J. Catal. 226 (2004) 466–470.
[23] J. Perez-Ramirez, M.S. Kumar, A. Bruckner, J. Catal. 223 (2004) 13–27.
[24] J. Perez-Ramirez, J. Catal. 227 (2004) 512–522.
[25] M.S. Kumar, M. Schwidder, W. Grünert, A. Brückner, J. Catal. 227 (2004) 384–397.
[26] G.D. Pirngruber, P.K. Roy, R. Prins, Phys. Chem. Chem. Phys. 8 (2006) 3939–3950.
[27] G.D. Pirngruber, P.K. Roy, N. Weiher, J. Phys. Chem. B 108 (2004) 13746–13754.
[28] W.M. Heijboer, D.C. Koningsberger, B.M. Weckhuysen, F.M.F. De Groot, Catal. Today 110 (2005) 228–238.
[29] A.A. Battiston, J.H. Bitter, W.M. Heijboer, F.M.F. De Groot, D.C. Koningsberger, J. Catal. 215 (2003) 279–293.
[30] A.A. Battiston, J.H. Bitter, D.C. Koningsberger, J. Catal. 218 (2003) 163–177.
[31] E.J.M. Hensen, Q. Zhu, R.A. van Santen, J. Catal. 220 (2003) 260–264.
[32] J. Perez-Ramirez, E.V. Kondratenko, Chem. Commun. 9 (2003) 2152–2153.
[33] J. Perez-Ramirez, A. Gallardo-Llamas, J. Phys. Chem. B 109 (2005) 20529–20538.
[34] K. Jisa, J. Novakova, M. Schwarze, A. Vondrova, S. Sklenak, Z. Sobalik, J. Catal. 262 (2009) 27–34.
[35] E. Tabor, K. Zaveta, N.K. Sathu, A. Vondrova, P. Sazama, Z. Sobalik, Catal. Today 175 (2011) 238–244.
[36] S. Sklenak, P.C. Andrikopoulos, B. Boekfa, B. Jansang, J. Novakova, L. Benco, T. Bucko, J. Hafner, J. Ddeek, Z. Sobalik, J. Catal. 272 (2010) 262–274.
[37] F. Kapteijn, G. Marban, J. Rodriguez-Mirasol, J.A. Moulijn, J. Catal. 167 (1997) 256–265.
[38] M. Iwasaki, K. Yamazaki, K. Banno, H. Shinjoh, J. Catal. 260 (2008) 205–216.
[39] R. Joyner, M. Stockenhuber, J. Phys. Chem. B 103 (1999) 5963–5976.
[40] R.W. Joyner, M. Stockenhuber, Catal. Lett. 45 (1997) 15–19.
[41] T.V. Voskoboinikov, H.Y. Chen, W.M.H. Sachtler, Appl. Catal. B: Environ. 19 (1998) 279–287.
[42] S. Brandenberger, O. Krocher, A. Tissler, R. Althoff, Catal. Rev. – Sci. Eng. 50 (2008) 492–531.
[43] A.A. Battiston, J.H. Bitter, D.C. Koningsberger, Catal. Lett. 66 (2000) 75–79.
[44] M. Melnik, M. Kohutova, Cent. Eur. J. Chem. 8 (2010) 965–991.
[45] H.Y. Chen, X. Wang, W.M.H. Sachtler, Appl. Catal. A: Gen. 194 (2000) 159–168.
[46] C.M. Flynn Jr, Chem. Rev. 84 (1984) 31–41.
[47] K. Lazar, G. Lejeune, R.K. Ahedi, S.S. Shevade, A.N. Kotasthane, J. Phys. Chem. B 102 (1998) 4865–4870.
[48] P. Fejes, J.B. Nagy, K. Lazar, J. Halasz, Appl. Catal. A: Gen. 190 (2000) 117–135.
[49] P. Fejes, I. Kiricsi, K. Lazar, I. Marsi, A. Rockenbauer, L. Korecz, J.B. Nagy, R. Aiello, F. Testa, Appl. Catal. A: Gen. 242 (2003) 247–266.
[50] E. Kuzmann, S. Nagy, A. Vertes, Pure Appl. Chem. 75 (2003) 801–858.
[51] A.R. Overweg, M.W.J. Craje, A.M. van der Kraan, I. Arends, A. Ribera, R.A. Sheldon, J. Catal. 223 (2004) 262–270.
[52] L. Guczi, K. Lazar, React. Kinet. Catal. Lett. 96 (2009) 335–343.
[53] S.M. Maier, A. Jentys, E. Metwalli, P. Muller-Buschbaum, J.A. Lercher, J. Phys. Chem. Lett. 2 (2011) 950–955.
[54] E. Tabor, K. Zaveta, N.K. Sathu, Z. Tvaruzkova, Z. Sobalik, Catal. Today 169 (2011) 16–23.
[55] B. Wichterlova, Z. Tvaruzkova, Z. Sobalik, P. Sarv, Microporous Mesoporous Mater. 24 (1998) 223–233.
[56] A. Zecchina, S. Bordiga, G. Spoto, D. Scarano, G. Petrini, G. Leofanti, M. Padovan, C.O. Arean, J. Chem. Soc. – Faraday Trans. 88 (1992) 2959–2969.
[57] R. Kefirov, E. Ivanova, K. Hadjiivanov, S. Dzwigaj, M. Che, Catal. Lett. 125 (2008) 209–214.
[58] P. Sazama, B. Wichterlova, J. Dedecek, Z. Tvaruzkova, Z. Musilova, L. Palumbo, S. Sklenak, O. Gonsiorova, Microporous Mesoporous Mater. 143 (2011) 87–96.
[59] L. Capek, J. Dedecek, P. Sazama, B. Wichterlova, J. Catal. 272 (2010) 44–54.
[60] L.J. Lobree, I.-C. Hwang, J.A. Reimer, A.T. Bell, J. Catal. 186 (1999) 242–253.
[61] K. Krishna, M. Makkee, Catal. Today 114 (2006) 23–30.
[62] G. Fierro, G. Moretti, G. Ferraris, G.B. Andreozzi, Appl. Catal. B: Environ. 102 (2011) 215–223.
[63] M. Mihaylov, E. Ivanova, K. Chakarova, P. Novachka, K. Hadjiivanov, Appl. Catal. A: Gen. 391 (2011) 3–10.
[64] V. Blasin-Aube, O. Marie, J. Saussey, A. Plesniar, M. Daturi, N. Nguyen, C. Hamon, M. Mihaylov, E. Ivanova, K. Hadjiivanov, J. Phys. Chem. C 113 (2009) 8387–8393.
[65] J. Dedecek, D. Kaucky, B. Wichterlova, Microporous Mesoporous Mater. 35–36 (2000) 483–494.
[66] J. Dedecek, Z. Sobalik, B. Wichterlova, Catal. Rev. – Sci. Eng. 54 (2012) 135–223.
[67] D. Kaucky, J. Dedecek, B. Wichterlova, Microporous Mesoporous Mater. 31 (1999) 75–87.
[68] Z. Sobalik, J. Novakova, J. Dedecek, N.K. Sathu, E. Tabor, P. Sazama, P. Stastny, B. Wichterlova, Microporous Mesoporous Mater. 146 (2011) 172–183.
[69] K. Lazar, O. Pozdnyakova, A. Wootsch, P. Fejes, Hyperfine Interact. 167 (2006) 779–784.
[70] J.B. Taboada, E.J.M. Hensen, I. Arends, G. Mul, A.R. Overweg, Catal. Today 110 (2005) 221–227.
[71] J. Perez-Ramirez, G. Mul, F. Kapteijn, J.A. Moulijn, A.R. Overweg, A. Domenech, A. Ribera, I.W.C.E. Arends, J. Catal. 207 (2002) 113–126.

[72] R.G. Burns, Hyperfine Interact. 91 (1994) 739–745.

[73] L. Capek, V. Kreibich, J. Dedecek, T. Grygar, B. Wichterlova, Z. Sobalik, J.A. Martens, R. Brosius, V. Tokarova, Microporous Mesoporous Mater. 80 (2005) 279–289.

[74] A.B.P. Lever, Inorganic Electron Spectroscopy, Elsevier, Amsterdam, 1968.

[75] J.P. Lange, K. Klier, Zeolites 14 (1994) 462–468.

[76] S. Bordiga, R. Buzzoni, F. Geobaldo, C. Lamberti, E. Giamello, A. Zecchina, G. Leofanti, G. Petrini, G. Tozzola, G. Vlaic, J. Catal. 158 (1996) 486–501.

[77] D.G. Barton, M. Shtein, R.D. Wilson, S.L. Soled, E. Iglesia, J. Phys. Chem. B 103 (1999) 630–640.

[78] D. Kaucky, B. Wichterlova, J. Dedecek, Z. Sobalik, I. Jakubec, Appl. Catal. A: Gen. 397 (2011) 82–93.

[79] J. Kiwi, N. Denisov, Y. Gak, N. Ovanesyan, P.A. Buffat, E. Suvorova, F. Gostev, A. Titov, O. Sarkisov, P. Albers, V. Nadtochenko, Langmuir 18 (2002) 9054–9066.

[80] B. Wichterlova, N. Zilkova, E. Uvarova, J. Cejka, P. Sarv, C. Paganini, J.A. Lercher, Appl. Catal. A: Gen. 182 (1999) 297–308.

[81] L. Palumbo, F. Bonino, P. Beato, M. Bjorgen, A. Zecchina, S. Bordiga, J. Phys. Chem. C 112 (2008) 9710–9716.

[82] S.S. Masiero, N.R. Marcilio, O.W. Perez-Lopez, Catal. Lett. 131 (2009) 194–202.

[83] I. Jirka, P. Sazama, A. Zikanova, P. Hrabanek, M. Kocirik, Microporous Mesoporous Mater. 137 (2011) 8–17.

[84] C.F. Baes, R.E. Mesmer, The Hydrolysis of Cations, Wiley, New York, 1976.

[85] Z. Sobalik, K. Jisa, H. Jirglova, B. Bernauer, Catal. Today 126 (2007) 73–80.

[86] P. Sazama, J. Dedecek, V. Gabova, B. Wichterlova, G. Spoto, S. Bordiga, J. Catal. 254 (2008) 180–189.

[87] S. Brandenberger, O. Krocher, M. Casapu, A. Tissler, R. Althoff, Appl. Catal. B: Environ. 101 (2011) 649–659.

[88] P. Marturano, L. Drozdova, A. Kogelbauer, R. Prins, J. Catal. 192 (2000) 236–247.

[89] V.S. Chernyavsky, L.V. Pirutko, A.K. Uriarte, A.S. Kharitonov, G.I. Panov, J. Catal. 245 (2007) 466–469.

[90] W.M. Heijboer, A.A. Battiston, A. Knop-Gericke, M. Havecker, H. Bluhm, B.M. Weckhuysen, D.C. Koningsberger, F.M.F. De Groot, Phys. Chem. Chem. Phys. 5 (2003) 4484–4491.

[91] S.M. Maier, A. Jentys, M. Janousch, J.A. Van Bokhoven, J.A. Lercher, J. Phys. Chem. C 116 (2012) 5846–5856.

[92] S. Brandenberger, O. Krocher, A. Tissler, R. Althoff, Ind. Eng. Chem. Res. 50 (2011) 4308–4319.

[93] P.K. Roy, R. Prins, G.D. Pirngruber, Appl. Catal. B: Environ. 80 (2008) 226–236.

[94] D. Kaucky, Z. Sobalik, M. Schwarze, A. Vondrova, B. Wichterlova, J. Catal. 238 (2006) 293–300.

[95] J. Perez-Ramirez, A. Gallardo-Llamas, Appl. Catal. A: Gen. 279 (2005) 117–123.

[96] E.J.M. Hensen, Q. Zhu, R.A. Van Santen, J. Catal. 233 (2005) 136–146.

[97] A. Ates, C. Hardacre, A. Goguet, Appl. Catal. A: Gen. 441–442 (2012) 30–41.